

# Hypergeometric Shell Model

Mark Drela

MIT Department of Aeronautics & Astronautics

2 Aug 2019

## Contents

<b>1</b>	<b>Method Overview</b>	<b>4</b>
<b>2</b>	<b>Geometry</b>	<b>5</b>
<b>3</b>	<b>Stress Resultant Integrals</b>	<b>5</b>
3.1	Resultant Definitions . . . . .	5
3.2	Thin-Shell Approximations . . . . .	6
3.3	Stress Tensor Decomposition . . . . .	7
<b>4</b>	<b>Shell Momentum Equations</b>	<b>8</b>
4.1	Local Momentum Conservation . . . . .	8
4.2	Weighted-Residual Shell Momentum Equations . . . . .	8
<b>5</b>	<b>Surface Coordinates</b>	<b>9</b>
5.1	Basis Vectors . . . . .	9
5.2	Tangential Gradient . . . . .	10
<b>6</b>	<b>Strains</b>	<b>10</b>
6.1	Strain Tensor Decomposition . . . . .	10
6.2	In-Surface Strain Tensor . . . . .	10
6.3	Transverse Strains . . . . .	11
<b>7</b>	<b>Constitutive Relations</b>	<b>11</b>
7.1	Stress-Strain Relations . . . . .	11
7.2	Shell Stiffnesses . . . . .	12
<b>8</b>	<b>Finite-Element Solution</b>	<b>13</b>
8.1	Global Data . . . . .	13
8.2	Nodal Data . . . . .	14
8.2.1	Parameters . . . . .	14
8.2.2	Unknowns (primary variables) . . . . .	15
8.3	Element Interpolation . . . . .	15
8.3.1	Bilinear interpolation . . . . .	15
8.3.2	Biquadratic (HSM) interpolation . . . . .	16

8.3.3	Membrane and bending strain interpolation . . . . .	18
8.3.4	Director lean interpolations . . . . .	19
8.3.5	Rotated nodal data . . . . .	19
8.3.6	Interpolated data . . . . .	21
8.3.7	Strains and stresses . . . . .	22
8.3.8	Other derived data . . . . .	23
8.4	Equation Residuals . . . . .	24
8.4.1	Residual weights and integration . . . . .	24
8.4.2	Momentum residuals . . . . .	25
8.4.3	Angular momentum residuals . . . . .	25
8.5	Edge Loading Boundary Conditions . . . . .	25
8.5.1	Edge interpolation . . . . .	26
8.5.2	Loading boundary condition axes . . . . .	26
8.5.3	Edge loading boundary condition data . . . . .	27
8.6	Variable and Residual Projection Vectors . . . . .	28
8.6.1	Projection vector definitions . . . . .	28
8.6.2	Variable projection . . . . .	29
8.6.3	Residual projection . . . . .	30
8.7	Geometry Boundary Conditions . . . . .	30
8.7.1	Dirichlet boundary condition data . . . . .	30
8.7.2	Target equations for Dirichlet boundary conditions . . . . .	30
8.8	Node Joining Conditions . . . . .	31
8.8.1	Force and position matching . . . . .	32
8.8.2	Moment and angle matching . . . . .	33
<b>9</b>	<b>Newton Solution</b>	<b>33</b>
<b>10</b>	<b>Unsteady Extension</b>	<b>35</b>
10.1	Unsteady Variables and Equations . . . . .	35
10.2	Time-Marching . . . . .	36
10.3	Perturbation Analysis . . . . .	36
10.3.1	Bode analysis . . . . .	36
10.3.2	Eigenmode analysis . . . . .	37
<b>11</b>	<b>Post-Processing Calculations</b>	<b>37</b>
11.1	Deformed-Geometry Nodal Basis Vectors . . . . .	38
11.2	Nodal Strain and Stress Resultants . . . . .	39

11.3 Maximum Strain and Stress . . . . .	41
<b>12 Stiffness Matrix Specification</b>	<b>42</b>
12.1 General and shell constitutive relations . . . . .	42
12.2 Isotropic material properties . . . . .	42
12.3 Orthotropic material properties . . . . .	43
12.4 Resultant stiffness matrix calculation . . . . .	43
12.5 Lumped-structure shells . . . . .	43

# 1 Method Overview

The earliest numerical solutions of shell problems with general geometry treated the shell elements as degenerate 3D solids, such as the pioneering work of Ahmad, Irons, and Zienkewicz [1]. These circumvented the complexity of global curvilinear coordinates [2] by formulating the problem in 3D cartesian space with the node position vectors  $\mathbf{r}$  as primary unknowns, and with the transverse material fiber direction represented by a material quasi-normal vector (or director)  $\hat{\mathbf{d}}$  which is another primary unknown. However, the early formulations suffered from shear locking, where the transverse shear strains resulting from the  $\mathbf{r}$  and  $\hat{\mathbf{d}}$  fields could not be correctly represented in the thin-shell limit. Large solid-body rotations were also not captured exactly.

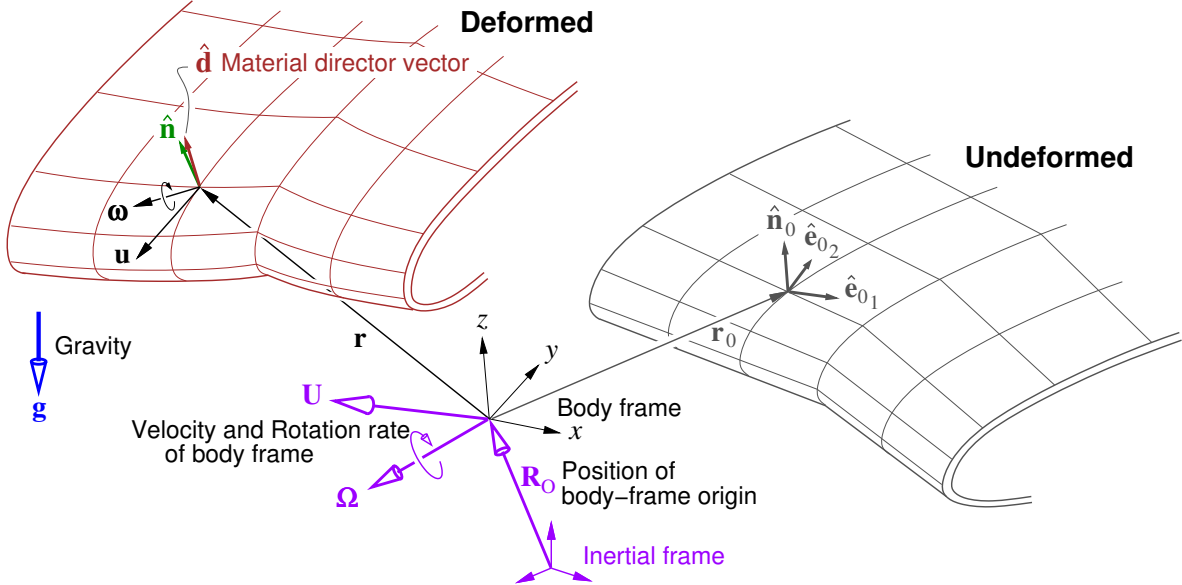


Figure 1: Shell geometry defined by deformed and undeformed position vectors  $\mathbf{r}, \mathbf{r}_0$  relative to body frame. Anisotropic shell properties are defined along local  $\hat{\mathbf{e}}_1, \hat{\mathbf{e}}_2, \hat{\mathbf{n}}$  basis vectors. Shell velocity  $\mathbf{u}$  and rotation rate  $\boldsymbol{\omega}$  relative to body frame, and body-frame velocity  $\mathbf{U}(t)$  and rotation rate  $\boldsymbol{\Omega}(t)$  relative to some inertial frame are used in dynamic problems. All vectors are defined via components along global  $xyz$  axes.

More recent shell mode developments, such as those of Dvorkin and Bathe[3], sidestep the shear locking problem by representing the transverse shear stress field indirectly via a special interpolation scheme from the edge midpoints (not nodes) of a quadrilateral element. The further development of Simo et al [4],[5] further refined this model with a geometrically-exact treatment valid for large shell curvatures. Talamini [6] developed a Discontinuous-Galerkin version applicable to quad or triangular elements. Ibrahimbegović[7] formulated a similar with an added drilling degrees of freedom.

The present Hypergeometric Shell Model (HSM) combines the existing shell methods with a higher-order treatment of the local shell curvatures, and also includes local drilling rotation angles for a higher-order treatment of the membrane strain field. The stiffness properties are defined in the local orthonormal basis formed by the undeformed geometry's normal vector  $\hat{\mathbf{n}}_0$  and in-surface vectors  $\hat{\mathbf{e}}_1, \hat{\mathbf{e}}_2$ . The latter can have any orientation, thus simplifying the specification of anisotropic materials independently of the discretization. The corresponding  $\hat{\mathbf{n}}, \hat{\mathbf{e}}_1, \hat{\mathbf{e}}_2$  of the deformed geometry are also computed, and serve as the basis for the vector and tensor outputs of the solution.

## 2 Geometry

The reference surface (e.g. inner, interior, or outer surface) of the deformed shell geometry is defined by the body-frame position vector  $\mathbf{r}(\xi, \eta)$ , while the specified undeformed geometry is defined by  $\mathbf{r}_0(\xi, \eta)$ . The third material coordinate  $\zeta$  is defined normal to the undeformed reference surface, but will tilt off-normal in the presence of transverse shear strains.

As in most other shell methods, a primary unknown in HSM is the quasi-normal vector (or director)  $\hat{\mathbf{d}}_{(\xi, \eta)}$  which lies along the material coordinate  $\zeta$ , and gives the position  $\mathbf{r}'$  of a general point off the reference surface.

$$\mathbf{r}'_{(\xi, \eta, \zeta)} = \mathbf{r} + \zeta \hat{\mathbf{d}} \quad (1)$$

The position, velocity, and acceleration of the reference-surface material point  $\mathbf{r}$  relative to the inertial earth frame are

$$\mathbf{R} = \mathbf{R}_B + \mathbf{r} \quad (2)$$

$$\mathbf{V} = \mathbf{U} + \mathbf{u} + \boldsymbol{\Omega} \times \mathbf{r} \quad (3)$$

$$\mathbf{a} = \dot{\mathbf{U}} + \dot{\mathbf{u}} + \dot{\boldsymbol{\Omega}} \times \mathbf{r} + \boldsymbol{\Omega} \times \dot{\mathbf{r}} + \boldsymbol{\Omega} \times \mathbf{V} \quad (4)$$

$$= \dot{\mathbf{U}} + \boldsymbol{\Omega} \times \mathbf{U} + \dot{\mathbf{u}} + \dot{\boldsymbol{\Omega}} \times \mathbf{r} + \boldsymbol{\Omega} \times (\boldsymbol{\Omega} \times \mathbf{r}) + 2\boldsymbol{\Omega} \times \mathbf{u} \quad (5)$$

where  $\mathbf{u} = \dot{\mathbf{r}}$  is the velocity of point  $\mathbf{r}$  in the  $xyz$  body frame. The absolute position, velocity, and acceleration of the general point  $\mathbf{r}'$  off the reference surface are in turn given by

$$\mathbf{R}' = \mathbf{R} + \zeta \hat{\mathbf{d}} \quad (6)$$

$$\mathbf{V}' = \mathbf{V} + \zeta \mathbf{V}_\zeta \quad (7)$$

$$\mathbf{a}' = \mathbf{a} + \zeta \mathbf{a}_\zeta \quad (8)$$

$$\mathbf{V}_\zeta \equiv (\boldsymbol{\Omega} + \boldsymbol{\omega}) \times \hat{\mathbf{d}} \quad (9)$$

$$\mathbf{a}_\zeta \equiv (\dot{\boldsymbol{\Omega}} + \dot{\boldsymbol{\omega}}) \times \hat{\mathbf{d}} + \boldsymbol{\Omega} \times (\boldsymbol{\Omega} \times \hat{\mathbf{d}}) + \boldsymbol{\omega} \times (\boldsymbol{\omega} \times \hat{\mathbf{d}}) + 2\boldsymbol{\Omega} \times (\boldsymbol{\omega} \times \hat{\mathbf{d}}) \quad (10)$$

where  $\boldsymbol{\omega} = \hat{\mathbf{d}} \times \dot{\hat{\mathbf{d}}} + \hat{\mathbf{d}} \dot{\psi}$  is the rotation rate vector of the reference-surface-point  $\mathbf{r}$  relative to the body frame, and  $\mathbf{V}_\zeta$  and  $\mathbf{a}_\zeta$  are the transverse velocity and acceleration gradients.

## 3 Stress Resultant Integrals

### 3.1 Resultant Definitions

The integral linear and angular momentum equations for a shell will involve the following mass, inertia, stress, and stress-moment resultant integrals over the shell thickness, which are then functions of the surface coordinates  $\xi, \eta$ .

$$\mu(\xi, \eta) \equiv \int_{\zeta_{\text{bot}}}^{\zeta_{\text{top}}} \rho \, d\zeta \quad , \quad \varsigma(\xi, \eta) \equiv \int_{\zeta_{\text{bot}}}^{\zeta_{\text{top}}} \rho \zeta \, d\zeta \quad , \quad \iota(\xi, \eta) \equiv \int_{\zeta_{\text{bot}}}^{\zeta_{\text{top}}} \rho \zeta^2 \, d\zeta \quad (11)$$

$$\bar{\mathbf{f}}_{(\xi, \eta)} \equiv \int_{\zeta_{\text{bot}}}^{\zeta_{\text{top}}} \bar{\boldsymbol{\sigma}} \, d\zeta \quad , \quad \bar{\mathbf{m}}_{(\xi, \eta)} \equiv \int_{\zeta_{\text{bot}}}^{\zeta_{\text{top}}} \bar{\boldsymbol{\sigma}} \zeta \, d\zeta \quad (12)$$

Note that  $\hat{\mathbf{d}} \times \bar{\mathbf{m}}$  is the actual conventional force-moment vector (per unit length).

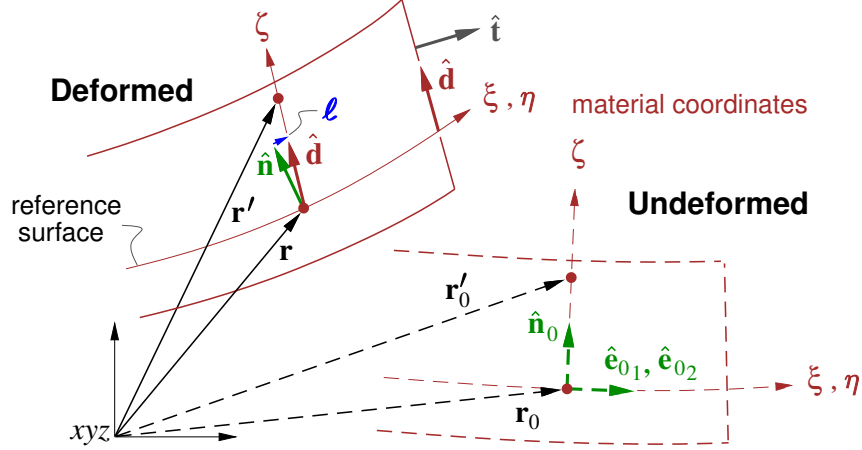


Figure 2: View through thickness of shell showing material-point position  $\mathbf{r}'$ , reference-surface position  $\mathbf{r}$ , and material quasi-normal  $\hat{\mathbf{d}}$ . Edge boundary conditions are defined using edge unit normal vector  $\hat{\mathbf{t}}$ .

A more exact treatment, such as that of Simo et al [4], defines the resultants implicitly by

$$\mu J = \int_{\zeta_{\text{bot}}}^{\zeta_{\text{top}}} \rho J' d\zeta, \quad \bar{\mathbf{f}} \cdot \mathbf{a}^\alpha J = \int_{\zeta_{\text{bot}}}^{\zeta_{\text{top}}} \bar{\boldsymbol{\sigma}} \cdot \mathbf{a}'^\alpha J' d\zeta, \quad \bar{\mathbf{m}} \cdot \mathbf{a}^\alpha J = \int_{\zeta_{\text{bot}}}^{\zeta_{\text{top}}} \bar{\boldsymbol{\sigma}} \cdot \mathbf{a}'^\alpha J' \zeta d\zeta \quad (13)$$

where the  $\mathbf{a}^\alpha$  ( $\alpha = 1, 2$ ) are the contravariant basis vectors normal to the  $\xi\zeta$  and  $\eta\zeta$  surfaces,  $J = \mathbf{a}_1 \times \mathbf{a}_2 \cdot \hat{\mathbf{d}}$  is the coordinate Jacobian, and  $(\cdot)'$  denotes a quantity off the  $\zeta = 0$  reference surface. The considerable complications of this more exact treatment will be avoided here by using the simpler definitions (12), which are seen to assume  $J' = J$  and  $\mathbf{a}' = \mathbf{a}$ .

At a shell element edge with unit edge-normal vector  $\hat{\mathbf{t}}$  as shown in Figure 3,  $\bar{\mathbf{f}} \cdot \hat{\mathbf{t}}$  is the overall edge traction force/length vector, and  $\hat{\mathbf{d}} \times \bar{\mathbf{m}} \cdot \hat{\mathbf{t}}$  is the edge bending moment/length vector. Also appearing will be the net top-bottom surface traction stress and stress-moment,

$$\mathbf{q}(\xi, \eta) \equiv \bar{\boldsymbol{\sigma}}_{\text{top}} \cdot \hat{\mathbf{n}}_{\text{top}} + \bar{\boldsymbol{\sigma}}_{\text{bot}} \cdot \hat{\mathbf{n}}_{\text{bot}} \quad (14)$$

$$\boldsymbol{\tau}(\xi, \eta) \equiv \zeta_{\text{top}} \bar{\boldsymbol{\sigma}}_{\text{top}} \cdot \hat{\mathbf{n}}_{\text{top}} + \zeta_{\text{bot}} \bar{\boldsymbol{\sigma}}_{\text{bot}} \cdot \hat{\mathbf{n}}_{\text{bot}} \quad (15)$$

although in the thin-shell limit the moment (per area)  $\boldsymbol{\tau}$  will be assumed negligible.

### 3.2 Thin-Shell Approximations

In the thin-shell approximation the shell thickness  $h$  is assumed to be much smaller than a typical shell dimension  $\ell$ , so that the shell is idealized as a surface with a vanishing thickness, as sketched in Figure 3.

$$\zeta_{\text{top}} - \zeta_{\text{bot}} \equiv h \ll \ell \quad (16)$$

One consequence is that the torques of linear and angular accelerations acting on the mass-moment and transverse moment of inertia can be assumed to be negligible.

$$\varsigma(\mathbf{g} - \mathbf{a}) \simeq \mathbf{0}, \quad \iota \dot{\boldsymbol{\omega}} \simeq \mathbf{0} \quad (17)$$

Furthermore, the transverse normal-stress resultant and all the transverse stress-moment resultants will have a negligible effect on the overall shell momentum balance, and can be dropped.

$$f_{nn} \simeq 0, \quad m_{1n}, m_{2n}, m_{nn} \simeq 0 \quad (18)$$

We will also assume that the shell thickness variations are small,  $|\tilde{\nabla}h| \ll 1$ , so that the top and bottom surface normal vectors are nearly anti-parallel, i.e.  $\hat{\mathbf{n}} = \hat{\mathbf{n}}_{\text{top}} = -\hat{\mathbf{n}}_{\text{bot}}$ . The loading (14) can then be defined using only the reference-surface normal vector  $\hat{\mathbf{n}}$ , and the moment loading (15) is assumed negligible.

$$\mathbf{q}(\xi, \eta) \simeq (\bar{\bar{\boldsymbol{\sigma}}}_{\text{top}} - \bar{\bar{\boldsymbol{\sigma}}}_{\text{bot}}) \cdot \hat{\mathbf{n}} \quad (19)$$

$$\boldsymbol{\tau}(\xi, \eta) \simeq \mathbf{0} \quad (20)$$

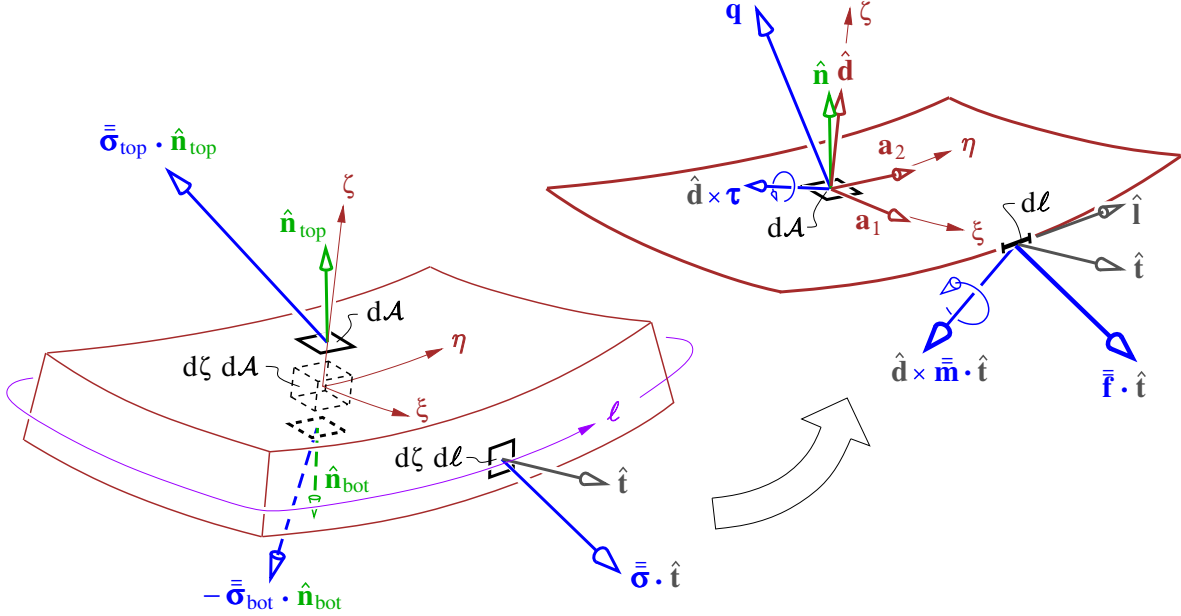


Figure 3: Shell element volume used to formulate integral momentum equations for the shell's idealized zero-thickness representation on the right. Tractions on volume surfaces become net force loading  $\mathbf{q}$  on the shell area and force loading  $\bar{\mathbf{f}} \cdot \hat{\mathbf{t}}$  and moment loading  $\hat{\mathbf{d}} \times \bar{\mathbf{m}} \cdot \hat{\mathbf{t}}$  on the shell edges. In-surface constitutive relations are defined along the in-surface basis vectors  $\hat{\mathbf{e}}_1, \hat{\mathbf{e}}_2$ . Discretization will be performed using local element coordinates  $\xi, \eta$ .

### 3.3 Stress Tensor Decomposition

The shell stiffness properties will be specified in the chosen local orthonormal  $\bar{\mathbf{e}}_0$  basis. The stress integral resultant tensor is therefore decomposed as

$$\bar{\bar{\mathbf{f}}} = \bar{\bar{\mathbf{f}}}_S + \bar{\bar{\mathbf{f}}}_T \quad (21)$$

where  $\bar{\bar{\mathbf{f}}}_S$  is the in-surface stress part and  $\bar{\bar{\mathbf{f}}}_T$  is the transverse shear-stress part. We then have

$$\bar{\bar{\mathbf{f}}}_S = f_{11} \hat{\mathbf{e}}_1 \hat{\mathbf{e}}_1 + f_{12} (\hat{\mathbf{e}}_1 \hat{\mathbf{e}}_2 + \hat{\mathbf{e}}_2 \hat{\mathbf{e}}_1) + f_{22} \hat{\mathbf{e}}_2 \hat{\mathbf{e}}_2 \quad (22)$$

$$\bar{\bar{\mathbf{f}}}_T = f_{1n} (\hat{\mathbf{e}}_1 \hat{\mathbf{n}} + \hat{\mathbf{n}} \hat{\mathbf{e}}_1) + f_{2n} (\hat{\mathbf{e}}_2 \hat{\mathbf{n}} + \hat{\mathbf{n}} \hat{\mathbf{e}}_2) \quad (23)$$

where each vector dyad denotes the usual outer product, i.e.  $\hat{\mathbf{e}}_1 \hat{\mathbf{e}}_2 = \hat{\mathbf{e}}_1 \hat{\mathbf{e}}_2^T = \hat{\mathbf{e}}_1 \otimes \hat{\mathbf{e}}_2$ . The remaining  $f_{nn} \hat{\mathbf{n}} \hat{\mathbf{n}}$  transverse normal-stress part is omitted, since this is assumed negligible within the thin-shell approximations.

The stress-moment integral resultant tensor is assumed to have the form

$$\bar{\mathbf{m}} = \bar{\mathbf{m}}_S = m_{11} \hat{\mathbf{e}}_1 \hat{\mathbf{e}}_1 + m_{12} (\hat{\mathbf{e}}_1 \hat{\mathbf{e}}_2 + \hat{\mathbf{e}}_2 \hat{\mathbf{e}}_1) + m_{22} \hat{\mathbf{e}}_2 \hat{\mathbf{e}}_2 \quad (24)$$

from which  $m_{1n}, m_{2n}, m_{nn}$  are omitted since these are negligible within the thin-shell approximation. The subscript on  $\bar{\mathbf{m}}_S$  is therefore superfluous.

## 4 Shell Momentum Equations

### 4.1 Local Momentum Conservation

The starting point for the discrete formulation is the 3D momentum equation for a material with Cauchy stress tensor  $\bar{\boldsymbol{\sigma}}$ , density  $\rho$ , acceleration  $\mathbf{a}'$ , and gravity  $\mathbf{g}$ .

$$\nabla \cdot \bar{\boldsymbol{\sigma}} + \rho(\mathbf{g} - \mathbf{a}') = \mathbf{0} \quad (25)$$

Forming  $\mathbf{r}' \times \{\text{eq.}(25)\}$ , using the identity

$$\mathbf{r}' \times \nabla \cdot \bar{\boldsymbol{\sigma}} = \nabla \cdot (\mathbf{r}' \times \bar{\boldsymbol{\sigma}}) + (\bar{\boldsymbol{\sigma}} \cdot \nabla) \times \mathbf{r}' \quad (26)$$

and the fact that  $\bar{\boldsymbol{\sigma}} = \bar{\boldsymbol{\sigma}}^T$  and  $\nabla \mathbf{r}' = \bar{\mathbf{I}}$  which make the last term in (26) zero, gives the divergence form of the angular momentum equation.

$$\nabla \cdot (\mathbf{r}' \times \bar{\boldsymbol{\sigma}}) + \rho \mathbf{r}' \times (\mathbf{g} - \mathbf{a}') = \mathbf{0} \quad (27)$$

### 4.2 Weighted-Residual Shell Momentum Equations

The integral shell momentum equations are obtained by multiplying equations (25) and (27) by the weighting function  $W_{(\xi, \eta)}$  which is nonzero only over a finite element such as the one shown in Figure 3. We then combine  $W$  with the divergence term, set  $\mathbf{r}' = \mathbf{r} + \zeta \hat{\mathbf{d}}$  and  $\mathbf{a}' = \mathbf{a} + \zeta \mathbf{a}_\zeta$ , and integrate over the element volume.

$$\iiint \left\{ \nabla \cdot (\bar{\boldsymbol{\sigma}} W) - \bar{\boldsymbol{\sigma}} \cdot \nabla W + \rho(\mathbf{g} - \mathbf{a}') W \right\} dV = \mathbf{0} \quad (28)$$

$$\iiint \left\{ \nabla \cdot [(\mathbf{r} + \zeta \hat{\mathbf{d}}) \times \bar{\boldsymbol{\sigma}} W] - (\mathbf{r} + \zeta \hat{\mathbf{d}}) \times \bar{\boldsymbol{\sigma}} \cdot \nabla W + \rho(\mathbf{r} + \zeta \hat{\mathbf{d}}) \times (\mathbf{g} - \mathbf{a}') W \right\} dV = \mathbf{0} \quad (29)$$

The first pure divergence volume integrals are next replaced by area integrals over the perimeter surface with surface-tangent vector  $\hat{\mathbf{t}}$  and area elements  $d\zeta d\ell$ , and over the top/bottom surfaces with normals  $\pm \hat{\mathbf{n}}$  and area elements  $d\mathcal{A}$ . For the remaining volume integrals the volume element is written as  $dV = d\zeta d\mathcal{A}$ .

We next introduce the tangential gradient which excludes any normal component along  $\hat{\mathbf{n}}$ ,

$$\tilde{\nabla} W_i \equiv \nabla W_i - (\hat{\mathbf{n}} \cdot \nabla W_i) \hat{\mathbf{n}} \quad (30)$$

as shown in Figure 4. We can then decompose the second stress terms in (28) and (29) as

$$\bar{\boldsymbol{\sigma}} \cdot \nabla W = \bar{\boldsymbol{\sigma}} \cdot \tilde{\nabla} W + (\hat{\mathbf{n}} \cdot \nabla W_i) \bar{\boldsymbol{\sigma}} \cdot \hat{\mathbf{n}} \quad (31)$$

and we note that the normal components will be very small for thin shells.

The integrations  $\int d\zeta$  across the shell thickness are now carried out, and the  $\mathbf{q}$  and  $\boldsymbol{\tau}$  definitions (19) are used for the top and bottom surface terms. The fact that  $W_{(\xi, \eta)}$  is defined to not vary in  $\zeta$



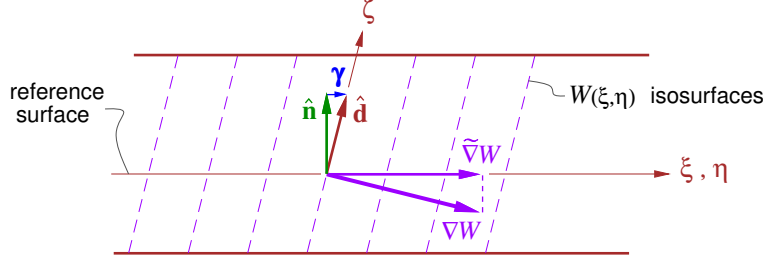


Figure 4: Weighting function gradient  $\nabla W_i$  and tangential gradient  $\tilde{\nabla} W_i$ , viewed through the shell thickness.

enables it to be put outside the  $\int d\zeta$  thickness integrals, so that the  $\mu, \varsigma, \bar{\mathbf{f}}, \bar{\mathbf{m}}$  definitions (12) and (12) can also be invoked. With the choice for  $W$  to be the specific  $W_i$  associated with some node  $i$ , equations (28) and (29) then become the linear and angular momentum residual vectors for that node.

$$\begin{aligned} \mathcal{R}_i^f \equiv & \oint \bar{\mathbf{f}} \cdot \hat{\mathbf{t}} W_i d\ell + \iint -\bar{\mathbf{f}} \cdot \tilde{\nabla} W_i d\mathcal{A} \\ & + \iint \left[ \mathbf{q} + \mu(\mathbf{g} - \mathbf{a}) - \varsigma \mathbf{a}_\zeta \right] W_i d\mathcal{A} = \mathbf{0} \end{aligned} \quad (32)$$

$$\begin{aligned} \mathcal{R}_i^m \equiv & \oint \left[ \hat{\mathbf{d}} \times \bar{\mathbf{m}} + \mathbf{r} \times \bar{\mathbf{f}} \right] \cdot \hat{\mathbf{t}} W_i d\ell + \iint -\left( \hat{\mathbf{d}} \times \bar{\mathbf{m}} + \mathbf{r} \times \bar{\mathbf{f}} \right) \cdot \nabla W_i d\mathcal{A} \\ & + \iint \left[ \hat{\mathbf{d}} \times \left( \boldsymbol{\tau} + \varsigma(\mathbf{g} - \mathbf{a}) - \iota \mathbf{a}_\zeta \right) + \mathbf{r} \times \left( \mathbf{q} + \mu(\mathbf{g} - \mathbf{a}) - \varsigma \mathbf{a}_\zeta \right) \right] W_i d\mathcal{A} = \mathbf{0} \end{aligned} \quad (33)$$

For thin shells the higher-moment  $\boldsymbol{\tau}, \varsigma, \iota$  terms above are very small and can be neglected, although retaining them causes no complications. Note also that in the absence of rotation, i.e.  $\boldsymbol{\Omega} = \boldsymbol{\omega} = \mathbf{0}$ , we have  $\mathbf{a}_\zeta = \mathbf{0}$ , in which case some of these terms vanish exactly.

## 5 Surface Coordinates

Quantities in the element surface coordinate basis will use traditional tensor index notation, with  $\xi, \eta$  denoted as  $\xi^1, \xi^2$ , or compactly as  $\xi^\alpha$  with  $\alpha \in \{1, 2\}$ . Coordinate derivatives will also be compactly denoted by  $\partial_\alpha(\cdot) \equiv \partial(\cdot)/\partial \xi^\alpha$ . Also following convention, vector and tensor covariant and contravariant components associated with these coordinates will be denoted by subscript and superscript indices, respectively. Vectors and tensors in boldface will indicate coordinate-independent (invariant) quantities, although in the numerical implementation they are defined via their global cartesian  $xyz$  components.

### 5.1 Basis Vectors

The covariant basis vectors are the  $\xi$  and  $\eta$  derivatives of the position vector  $\mathbf{r}(\xi, \eta)$ .

$$\mathbf{a}_\alpha(\xi, \eta) \equiv \partial_\alpha \mathbf{r} \quad (34)$$

These are then used to define the following surface metric, curvature, and director-lean tensors.

$$\check{g}_{\alpha\beta} \equiv \mathbf{a}_\alpha \cdot \mathbf{a}_\beta \quad (35)$$

$$\check{h}_{\alpha\beta} \equiv \mathbf{a}_\alpha \cdot \partial_\beta \hat{\mathbf{d}} \quad (36)$$

$$\check{\ell}_\alpha \equiv \mathbf{a}_\alpha \cdot \hat{\mathbf{d}} \quad (37)$$

The metric determinant and its inverse  $\check{g}^{\alpha\beta}$  are defined by

$$\check{g} \equiv \det(\check{g}_{\alpha\beta}) := \check{g}_{11}\check{g}_{22} - (\check{g}_{12})^2 = |\mathbf{a}_1 \times \mathbf{a}_2|^2 \quad (38)$$

$$\check{g}^{\alpha\beta} \equiv \left[ \check{g}_{\alpha\beta} \right]^{-1} = \frac{1}{\check{g}} \begin{bmatrix} \check{g}_{22} & -\check{g}_{12} \\ -\check{g}_{12} & \check{g}_{11} \end{bmatrix} \quad (39)$$

which then give the contravariant basis vectors and the area element.

$$\mathbf{a}^\alpha = \check{g}^{\alpha\beta} \mathbf{a}_\beta \quad (40)$$

$$d\mathcal{A} = \sqrt{\check{g}} d\xi^1 d\xi^2 \quad (41)$$

We also apply all the above definitions (34)–(40) to the undeformed geometry  $\mathbf{r}_0(\xi^\alpha)$ , to give the corresponding  $\mathbf{a}_{0\alpha}$ ,  $\check{g}_{0\alpha\beta}$ ,  $\check{h}_{0\alpha\beta}$ ,  $\check{\ell}_{0\alpha}$ ,  $\check{g}_0$ ,  $\check{g}_0^{\alpha\beta}$ , and  $\mathbf{a}_0^\alpha$ . The undeformed area element is  $d\mathcal{A}_0 = \sqrt{\check{g}_0} d\xi^1 d\xi^2$ .

## 5.2 Tangential Gradient

The tangential gradient of any scalar quantity on the surface is computed using its coordinate derivatives and the contravariant basis vectors.

$$\tilde{\nabla}_{()} = \mathbf{a}^1 \partial_{1()} + \mathbf{a}^2 \partial_{2()} \quad (42)$$

Gradients of in-surface vectors or tensors will not appear in the numerical solution method, which avoids the need to construct basis-vector gradients and associated Christoffel symbols.

## 6 Strains

### 6.1 Strain Tensor Decomposition

The strain tensor is decomposed as

$$\bar{\bar{\epsilon}} = \bar{\bar{\epsilon}}_S + \bar{\bar{\epsilon}}_T \quad (43)$$

where the in-surface part  $\bar{\bar{\epsilon}}_S$  contains only in-surface components, while the transverse part  $\bar{\bar{\epsilon}}_T$  contains all the normal components.

### 6.2 In-Surface Strain Tensor

The deformed and undeformed metric tensors give the Green strain tensor components of the reference surface in the element basis.

$$\check{\epsilon}_{\alpha\beta} \equiv \frac{1}{2} (\check{g}_{\alpha\beta} - \check{g}_{0\alpha\beta}) \quad (44)$$

For a point  $\mathbf{r}'$  at location  $\zeta$  from the reference surface  $\mathbf{r}(\xi^\alpha)$ , along the material quasi-normal vector  $\hat{\mathbf{d}}_{(\xi^\alpha)}$ , we have

$$\mathbf{r}'_{(\xi^\alpha, \zeta)} = \mathbf{r} + \zeta \hat{\mathbf{d}} \quad (45)$$

$$\partial_\alpha \mathbf{r}' = \mathbf{a}_\alpha + \zeta \partial_\alpha \hat{\mathbf{d}} \quad (46)$$

and the corresponding in-surface (at fixed  $\zeta$ ) metric off the reference surface is now

$$\begin{aligned}\check{g}'_{\alpha\beta} &\equiv \partial_\alpha \mathbf{r}' \cdot \partial_\beta \mathbf{r}' \\ &= \mathbf{a}_\alpha \cdot \mathbf{a}_\beta + 2\zeta \mathbf{a}_\alpha \cdot \partial_\beta \hat{\mathbf{d}} + \zeta^2 \partial_\alpha \hat{\mathbf{d}} \cdot \partial_\beta \hat{\mathbf{d}} \\ &\simeq \mathbf{a}_\alpha \cdot \mathbf{a}_\beta + 2\zeta \mathbf{a}_\alpha \cdot \partial_\beta \hat{\mathbf{d}} \quad (\zeta |\partial_\alpha \hat{\mathbf{d}}| \ll |\mathbf{a}_\alpha|) \end{aligned} \quad (47)$$

$$= \check{g}_{\alpha\beta} + 2\zeta \check{h}_{\alpha\beta} \quad (48)$$

where the approximate linearized form (47) or (48) is valid in the usual situation where the offset distance is much smaller than the shell's radii of curvature, as measured by  $\check{h}_{\alpha\beta}$ . The strain tensor off the reference surface is then

$$\begin{aligned}\check{\varepsilon}'_{\alpha\beta} &\equiv \frac{1}{2}(g'_{\alpha\beta} - g'_{0\alpha\beta}) \\ &= \check{\varepsilon}_{\alpha\beta} + \zeta \check{\kappa}_{\alpha\beta} \end{aligned} \quad (49)$$

$$\check{\kappa}_{\alpha\beta} \equiv \check{h}_{\alpha\beta} - \check{h}_{0\alpha\beta} \quad (50)$$

which is seen to have a membrane contribution  $\check{\varepsilon}_{\alpha\beta}$  due to tangential stretching and shearing of the reference surface, and a bending contribution  $\check{\kappa}_{\alpha\beta}$  due to curvature changes of the reference surface.

### 6.3 Transverse Strains

The transverse strain tensor is constructed using the deformed and undeformed director-lean components.

$$\check{\gamma}_\alpha \equiv \check{\ell}_\alpha - \check{\ell}_{0\alpha} \quad (51)$$

The invariant transverse shear strain vector is then

$$\boldsymbol{\gamma} = \check{\gamma}_\alpha \mathbf{a}^\alpha \quad (52)$$

$$:= \check{\gamma}_1 \mathbf{a}^1 + \check{\gamma}_2 \mathbf{a}^2 \quad (53)$$

and we can also define the complete invariant transverse shear strain tensor.

$$\bar{\bar{\varepsilon}}_T = \frac{1}{2} \check{\gamma}_\alpha (\mathbf{a}^\alpha \hat{\mathbf{n}} + \hat{\mathbf{n}} \mathbf{a}^\alpha) \quad (54)$$

$$:= \frac{1}{2} \check{\gamma}_1 (\mathbf{a}^1 \hat{\mathbf{n}} + \hat{\mathbf{n}} \mathbf{a}^1) + \frac{1}{2} \check{\gamma}_2 (\mathbf{a}^2 \hat{\mathbf{n}} + \hat{\mathbf{n}} \mathbf{a}^2) \quad (55)$$

## 7 Constitutive Relations

### 7.1 Stress-Strain Relations

The stress and strain tensors are related by assuming a Hookean material and introducing the stiffness tensors. The in-surface and transverse tensors are also assumed to be decoupled. When expressed in the local axes along  $\hat{\mathbf{e}}_{01}, \hat{\mathbf{e}}_{02}, \hat{\mathbf{n}}_0$ , the assumed constitutive laws are

$$\begin{Bmatrix} \sigma_{11} \\ \sigma_{22} \\ \sigma_{12} \end{Bmatrix} = \begin{bmatrix} c_{11} & c_{12} & c_{16} \\ \cdot & c_{22} & c_{26} \\ \cdot & \cdot & c_{66} \end{bmatrix} \begin{Bmatrix} \varepsilon'_{11} \\ \varepsilon'_{22} \\ \varepsilon'_{12} \end{Bmatrix} \quad (56)$$

$$\begin{Bmatrix} \sigma_{1n} \\ \sigma_{2n} \end{Bmatrix} = \begin{bmatrix} c_{55} & 0 \\ 0 & c_{44} \end{bmatrix} \begin{Bmatrix} \gamma'_1 \\ \gamma'_2 \end{Bmatrix} \quad (57)$$

in which the remaining normal stress  $\sigma_{nn}$  is assumed to be negligible, and the prime on  $\varepsilon'$  and  $\gamma'$  indicates strain at location  $\zeta$  off the reference surface. The indicated matrix symmetry is required for angular momentum conservation of an infinitesimal material volume.

The stiffness matrices are actually 4th-order tensors, but are written above in traditional Voigt notation which contracts pairs of indices as  $11 \rightarrow 1$ ,  $22 \rightarrow 2$ ,  $12 \rightarrow 6$ ,  $1n \rightarrow 5$ ,  $2n \rightarrow 4$ . The uncontracted forms will be more convenient when the tensors are converted to the element basis.

Following standard shell-theory approximations we assume that the transverse material lines remain straight, so that we can invoke (49) and write the in-surface strains as linear functions of  $\zeta$ ,

$$\begin{Bmatrix} \varepsilon'_{11}(\zeta) \\ \varepsilon'_{22}(\zeta) \\ \varepsilon'_{12}(\zeta) \end{Bmatrix} = \begin{Bmatrix} \varepsilon_{11} \\ \varepsilon_{22} \\ \varepsilon_{12} \end{Bmatrix} + \zeta \begin{Bmatrix} \kappa_{11} \\ \kappa_{22} \\ \kappa_{12} \end{Bmatrix} \quad (58)$$

where  $\kappa$  are components of the curvature-change tensor. The transverse shear strains  $\gamma'_1, \gamma'_2$  will have some more complicated  $\zeta$  dependence, since they must fall to zero at the top and bottom shell surface. Following shell theory we will replace them by the averages  $\gamma_1, \gamma_2$  independent of  $\zeta$ ,

$$\begin{Bmatrix} \gamma'_1(\zeta) \\ \gamma'_2(\zeta) \end{Bmatrix} = K \begin{Bmatrix} \gamma_1 \\ \gamma_2 \end{Bmatrix} \quad (59)$$

where  $K$  is the shear strain energy reduction factor. The commonly-chosen value  $K = 5/6$  corresponds to parabolic  $\gamma'_1(\zeta)$  and  $\gamma'_2(\zeta)$  across the shell thickness, which is the correct result for a uniform isotropic shell.

## 7.2 Shell Stiffnesses

We now substitute the strain components in (58) into the stress/strain relations (56),(57), and then insert that into the stress and stress-moment resultant definitions (12). This produces the following linear system which gives each in-surface stress resultant in terms of all the strain resultants.

$$\begin{Bmatrix} f_{11} \\ f_{22} \\ f_{12} \\ m_{11} \\ m_{22} \\ m_{12} \end{Bmatrix} = \left[ \begin{array}{ccc|ccc} A_{11} & A_{12} & A_{16} & B_{11} & B_{12} & B_{16} \\ \cdot & A_{22} & A_{26} & \cdot & B_{22} & B_{26} \\ \cdot & \cdot & A_{66} & \cdot & \cdot & B_{66} \\ \hline B_{11} & B_{12} & B_{16} & D_{11} & D_{12} & D_{16} \\ \cdot & B_{22} & B_{26} & \cdot & D_{22} & D_{26} \\ \cdot & \cdot & B_{66} & \cdot & \cdot & D_{66} \end{array} \right] \begin{Bmatrix} \varepsilon_{11} \\ \varepsilon_{22} \\ \varepsilon_{12} \\ \kappa_{11} \\ \kappa_{22} \\ \kappa_{12} \end{Bmatrix} \quad (60)$$

$$\begin{Bmatrix} f_{1n} \\ f_{2n} \end{Bmatrix} = \begin{bmatrix} S_{55} & 0 \\ 0 & S_{44} \end{bmatrix} \begin{Bmatrix} \gamma_1 \\ \gamma_2 \end{Bmatrix} \quad (61)$$

The stiffness submatrices above are defined by the following weighted integrals over the shell thick-

ness, which capture the overall lumped properties of the shell cross section.

$$\bar{\bar{A}} = \begin{bmatrix} A_{11} & A_{12} & A_{16} \\ \cdot & A_{22} & A_{26} \\ \cdot & \cdot & A_{66} \end{bmatrix} \equiv \int \begin{bmatrix} c_{11} & c_{12} & c_{16} \\ \cdot & c_{22} & c_{26} \\ \cdot & \cdot & c_{66} \end{bmatrix} d\zeta \quad (62)$$

$$\bar{\bar{B}} = \begin{bmatrix} B_{11} & B_{12} & B_{16} \\ \cdot & B_{22} & B_{26} \\ \cdot & \cdot & B_{66} \end{bmatrix} \equiv \int \begin{bmatrix} c_{11} & c_{12} & c_{16} \\ \cdot & c_{22} & c_{26} \\ \cdot & \cdot & c_{66} \end{bmatrix} \zeta d\zeta \quad (63)$$

$$\bar{\bar{D}} = \begin{bmatrix} D_{11} & D_{12} & D_{16} \\ \cdot & D_{22} & D_{26} \\ \cdot & \cdot & D_{66} \end{bmatrix} \equiv \int \begin{bmatrix} c_{11} & c_{12} & c_{16} \\ \cdot & c_{22} & c_{26} \\ \cdot & \cdot & c_{66} \end{bmatrix} \zeta^2 d\zeta \quad (64)$$

$$\bar{\bar{S}} = \begin{bmatrix} S_{55} & 0 \\ 0 & S_{44} \end{bmatrix} \equiv \frac{1}{K} \int \begin{bmatrix} c_{55} & 0 \\ 0 & c_{44} \end{bmatrix} d\zeta \quad (65)$$

In shell theory it is common to choose the reference surface to lie in the middle of the shell thickness, so that for a homogeneous shell material the  $\bar{\bar{B}}$  matrix elements in (63) are all zero, and the  $f$  and  $m$  components in the stiffness matrix equation (60) then decouple. Here no such assumption is made, to allow complete freedom in the choice of the reference surface location and of the shell composition.

## 8 Finite-Element Solution

As in the theory derivations, here the  $xyz$  vectors and tensors in the global cartesian basis will be written in boldface, the  $12n$  vectors and tensors in the  $\bar{\bar{\mathbf{e}}}$  basis will be denoted in italic, and the covariant  $\xi\eta$  vector and tensor components in the contravariant  $\mathbf{a}^\alpha$  basis will be in italic with a breve and with index subscripts, e.g.

$$\bar{\bar{\mathbf{e}}} \equiv \begin{bmatrix} \varepsilon_{xx} & \varepsilon_{xy} & \varepsilon_{xz} \\ \cdot & \varepsilon_{yy} & \varepsilon_{yz} \\ \cdot & \cdot & \varepsilon_{zz} \end{bmatrix}, \quad \bar{\bar{\mathbf{e}}} \equiv \begin{bmatrix} \varepsilon_{11} & \varepsilon_{12} & \varepsilon_{1n} \\ \cdot & \varepsilon_{22} & \varepsilon_{2n} \\ \cdot & \cdot & \varepsilon_{nn} \end{bmatrix}, \quad \check{\varepsilon}_{\alpha\beta} \equiv \begin{bmatrix} \check{\varepsilon}_{11} & \check{\varepsilon}_{12} \\ \cdot & \check{\varepsilon}_{22} \end{bmatrix}$$

Contravariant components in the covariant  $\mathbf{a}_\alpha$  basis will have superscripts, e.g.  $\check{f}^{\alpha\beta}$ .

### 8.1 Global Data

The global data is listed below. For stationary problems, the only global parameter is the gravity acceleration vector  $\mathbf{g}$ . For non-stationary problems, additional parameters would be the frame velocity  $\mathbf{U}(t)$  at the  $xyz$  origin and frame rotation rate  $\mathbf{\Omega}(t)$ , both sketched in Figure 1, and their corresponding rates  $\dot{\mathbf{U}}(t)$  and  $\dot{\mathbf{\Omega}}(t)$ , all relative to some inertial frame of reference (e.g. earth). These can be either prescribed, as in a forced-motion case, or evolved in time via additional kinematic constraints and global linear and angular momentum conservation constraints, as in a free-body case.

symbol	num.	axes	description
$\mathbf{g}$	3	$xyz$	gravity acceleration
$\mathbf{U}(t)$	3	$xyz$	frame velocity
$\mathbf{\Omega}(t)$	3	$xyz$	frame rotation rate
$\dot{\mathbf{U}}(t)$	3	$xyz$	frame velocity time rate of change
$\dot{\mathbf{\Omega}}(t)$	3	$xyz$	frame rotational acceleration

Note that the absolute linear acceleration of the  $xyz$  body frame's origin is

$$\mathbf{a}_B(t) = \dot{\mathbf{U}} + \mathbf{\Omega} \times \mathbf{U} \quad (66)$$

where the first term is the longitudinal component and the second term is the transverse (centripetal) component. A *static* problem is one where  $\mathbf{a}_B$  is constant in time, making the solution in the  $xyz$  frame steady. For a purely translating case, which has  $\mathbf{\Omega} = \dot{\mathbf{\Omega}} = \mathbf{0}$ , we can ignore  $\mathbf{U}$ . And in this case if  $\dot{\mathbf{U}}$  is also constant in time, it can be lumped into a modified effective gravity vector.

$$\mathbf{g} \leftarrow \mathbf{g} - \dot{\mathbf{U}}$$

## 8.2 Nodal Data

Each element corner node  $j$  has the parameter and variable data listed below. Bilinear interpolation to the element interior then makes these quantities functions of the  $(\xi, \eta)$  element coordinates as described above.

### 8.2.1 Parameters

These input quantities describe the undeformed shell geometry, structural properties, mass, and loading. They are all defined at each node  $j$ , and used either at the nodes to compute secondary variables, or interpolated to the element interior to construct the equation residuals.

symbol	num.	axes	description
$\mathbf{r}_{0j}$	3	$xyz$	position vector of undeformed geometry
$\bar{\mathbf{e}}_{0j}$	9	$xyz$	$\hat{\mathbf{e}}_{01}, \hat{\mathbf{e}}_{02}, \hat{\mathbf{n}}_0$ unit vectors of undeformed geometry
$\bar{\bar{A}}_j$	6	$12n$	lumped shell stiffness matrix (extension and shear stiffness)
$\bar{\bar{B}}_j$	6	$12n$	lumped shell stiffness matrix (extension/bending coupling)
$\bar{\bar{D}}_j$	6	$12n$	lumped shell stiffness matrix (bending stiffness)
$\bar{\bar{S}}_j$	2	$12n$	lumped shell stiffness matrix (transverse shear stiffness)
$q_{n_j}$	1	$12n$	shell-following applied normal force/area
$\mathbf{q}_{xyzj}$	3	$xyz$	fixed-direction applied force/area
$\mu_j$	1	—	lumped shell mass (mass/area density)

In practice, the undeformed geometry is defined by the parametric surface  $\mathbf{r}_0(u, v)$ , where  $u, v$  are the global (e.g. B-spline) surface coordinates. This also then uniquely defines the  $\hat{\mathbf{n}}(u, v)$  distribution.

$$\hat{\mathbf{n}}_0 = \frac{\partial_u \mathbf{r}_0 \times \partial_v \mathbf{r}_0}{|\partial_u \mathbf{r}_0 \times \partial_v \mathbf{r}_0|} \quad (67)$$

For isotropic shell materials, the  $\hat{\mathbf{e}}_{01}, \hat{\mathbf{e}}_{02}$  vectors are completely arbitrary, and can be conveniently

computed by evaluating

$$\hat{\mathbf{e}}_{01} = \frac{(1-t)\partial_u \mathbf{r}_0 + t\partial_v \mathbf{r}_0}{|(1-t)\partial_u \mathbf{r}_0 + t\partial_v \mathbf{r}_0|} \quad (68)$$

$$\hat{\mathbf{e}}_{02} = \hat{\mathbf{n}}_0 \times \hat{\mathbf{e}}_{01} \quad (69)$$

at each node, in which the constant  $t$  selects the azimuthal orientation of the  $\hat{\mathbf{e}}_{01}, \hat{\mathbf{e}}_{02}$  vectors within the surface; choosing  $t=0$  aligns  $\hat{\mathbf{e}}_{01}$  with  $\partial_u \mathbf{r}_0$ , and choosing  $t=1$  aligns  $\hat{\mathbf{e}}_{01}$  with  $\partial_v \mathbf{r}_0$ . If the shell material is e.g. orthotropic with known properties along specific axes, then it is most convenient to orient  $\hat{\mathbf{e}}_{01}, \hat{\mathbf{e}}_{02}$  along these axes, since this will then simplify the stiffness matrix specification.

An example of a shell-following normal load is the bottom/top pressure difference across the shell.

$$q_n = p_{\text{bot}} - p_{\text{top}} \quad (70)$$

A shell-following tangential load vector, such as skin friction, could also be specified.

### 8.2.2 Unknowns (primary variables)

These are the primary variables which are to be determined at each node  $j$ .

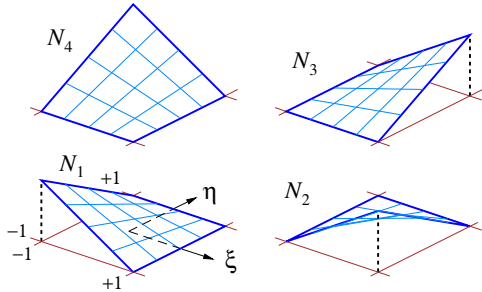
symbol	num.	axes	description
$\mathbf{r}_j$	3	$xyz$	position vector of deformed geometry
$\hat{\mathbf{d}}_j$	3	$xyz$	unit material quasi-normal vector of deformed geometry
$\psi_j$	1	—	drilling rotation angle

It should be noted that each  $\hat{\mathbf{d}}_j$  vector, since it has unit magnitude, actually represents two rather than three unknowns, which will be accounted for later in the Newton solution method formulation. The resulting numerical problem will then have a total of six unknowns per node.

## 8.3 Element Interpolation

### 8.3.1 Bilinear interpolation

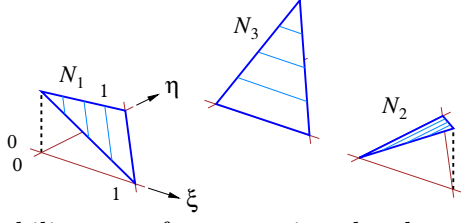
Per standard practice, these nodal quantities are interpolated over the element via four bilinear functions  $N_j(\xi, \eta)$ , using the normalized parameters  $-1 \leq \xi \leq +1$ ,  $-1 \leq \eta \leq +1$  spanning the cell.



$$\begin{aligned}
 N_1(\xi, \eta) &\equiv \frac{1}{4}(1-\xi)(1-\eta) \\
 N_2(\xi, \eta) &\equiv \frac{1}{4}(1+\xi)(1-\eta) \\
 N_3(\xi, \eta) &\equiv \frac{1}{4}(1+\xi)(1+\eta) \\
 N_4(\xi, \eta) &\equiv \frac{1}{4}(1-\xi)(1+\eta)
 \end{aligned} \quad (71)$$

A triangular element can also be used, and will have the following three linear interpolation func-

tions, defined over  $0 \leq \xi \leq 1$ ,  $0 \leq \eta \leq 1$ .



$$\begin{aligned} N_1(\xi, \eta) &\equiv 1 - \xi - \eta \\ N_2(\xi, \eta) &\equiv \xi \\ N_3(\xi, \eta) &\equiv \eta \end{aligned} \quad (72)$$

The bilinear surface spanning the element is defined by

$$\bar{\mathbf{r}}(\xi, \eta) = \sum_j \mathbf{r}_j N_j \quad (73)$$

where the sum runs over  $j = 1, 2, 3, 4$  or  $j = 1, 2, 3$ , depending on the type of element. Its directional derivatives are similarly constructed from the derivatives of the interpolation functions.

$$\partial_\alpha \bar{\mathbf{r}}(\xi, \eta) = \sum_j \mathbf{r}_j \partial_\alpha N_j \quad (74)$$

The director field is likewise interpolated from the nodes, with an additional normalization to preserve unit length.

$$\mathbf{d}(\xi, \eta) = \sum_j \hat{\mathbf{d}}_j N_j \quad (75)$$

$$\hat{\mathbf{d}}(\xi, \eta) = \frac{\mathbf{d}}{|\mathbf{d}|} \quad (76)$$

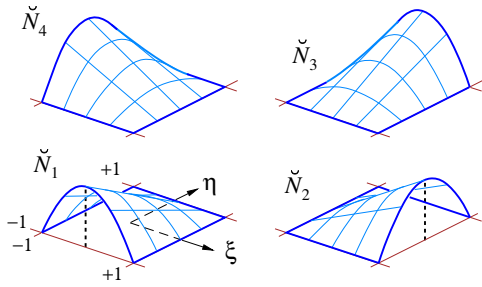
The derivatives then also follow.

$$\partial_\alpha \mathbf{d}(\xi, \eta) = \sum_j \hat{\mathbf{d}}_j \partial_\alpha N_j \quad (77)$$

$$\partial_\alpha \hat{\mathbf{d}}(\xi, \eta) = \frac{1}{|\mathbf{d}|} \left[ \partial_\alpha \mathbf{d} - \hat{\mathbf{d}} (\hat{\mathbf{d}} \cdot \partial_\alpha \mathbf{d}) \right] \quad (78)$$

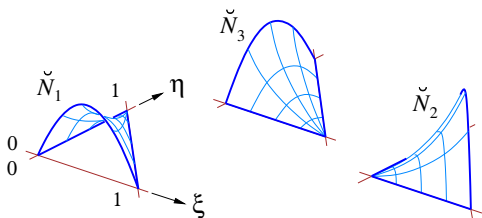
### 8.3.2 Biquadratic (HSM) interpolation

The higher-order geometry treatment of HSM is formulated using quadratic edge interpolation functions. For a quad element these are



$$\begin{aligned} \check{N}_1(\xi, \eta) &\equiv \frac{1}{8}(1 - \xi^2)(1 - \eta) \\ \check{N}_2(\xi, \eta) &\equiv \frac{1}{8}(1 - \eta^2)(1 + \xi) \\ \check{N}_3(\xi, \eta) &\equiv \frac{1}{8}(1 - \xi^2)(1 + \eta) \\ \check{N}_4(\xi, \eta) &\equiv \frac{1}{8}(1 - \eta^2)(1 - \xi) \end{aligned} \quad (79)$$

and for a triangle element they are



$$\begin{aligned} \check{N}_1(\xi, \eta) &\equiv \frac{1}{2}(1 - \xi - \eta) \xi \\ \check{N}_2(\xi, \eta) &\equiv \frac{\sqrt{2}}{2} \xi \eta \\ \check{N}_3(\xi, \eta) &\equiv \frac{1}{2} \eta (1 - \xi - \eta) \end{aligned} \quad (80)$$



where the numerical coefficients are chosen to make the edge directional derivatives in parameter space be equal to  $\pm \frac{1}{2}$  at the edge endpoints.

The higher-order geometry  $\mathbf{r}$  starts with the bilinear surface  $\bar{\mathbf{r}}$ , and adds a transverse quadratic “bubble” modification  $\Delta \mathbf{r}^N$  which has edge amplitudes  $B_j$ , and an in-surface quadratic “drilling” modification  $\Delta \mathbf{r}^S$  which has node amplitudes  $\psi_j$ .

$$\mathbf{r}(\xi, \eta) = \bar{\mathbf{r}} + \Delta \mathbf{r}^N + \Delta \mathbf{r}^S \quad (81)$$

$$\mathbf{a}_\alpha = \partial_\alpha \bar{\mathbf{r}} + \partial_\alpha \Delta \mathbf{r}^N + \partial_\alpha \Delta \mathbf{r}^S \quad (82)$$

$$\Delta \mathbf{r}^N(\xi, \eta) \equiv \sum_{\text{edges}} \hat{\mathbf{d}}(\xi, \eta) B_j \check{N}_j(\xi, \eta) \quad (83)$$

$$\Delta \mathbf{r}^S(\xi, \eta) \equiv \sum_{\text{nodes}} \psi_j \hat{\mathbf{d}}_j \times (\bar{\mathbf{r}}(\xi, \eta) - \mathbf{r}_j) N_j(\xi, \eta) \quad (84)$$

$$\partial_\alpha \Delta \mathbf{r}^N = \sum_{\text{edges}} B_j \left( \partial_\alpha \hat{\mathbf{d}} \check{N}_j + \hat{\mathbf{d}} \partial_\alpha \check{N}_j \right) \quad (85)$$

$$\partial_\alpha \Delta \mathbf{r}^S = \sum_{\text{nodes}} \psi_j \left( \hat{\mathbf{d}}_j \times \partial_\alpha \bar{\mathbf{r}} N_j + \hat{\mathbf{d}}_j \times (\bar{\mathbf{r}} - \mathbf{r}_j) \partial_\alpha N_j \right) \quad (86)$$

The contributions of these higher-order terms are diagrammed in Figures 5 and 6. Either (or both) can be omitted to revert the method to the standard bilinear formulation.

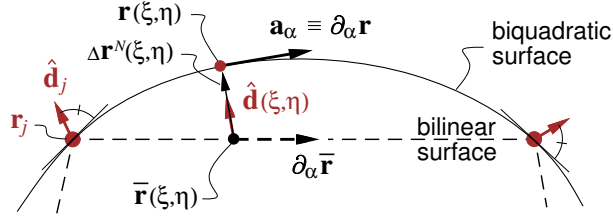


Figure 5: Transverse higher-order correction to bilinear geometry.

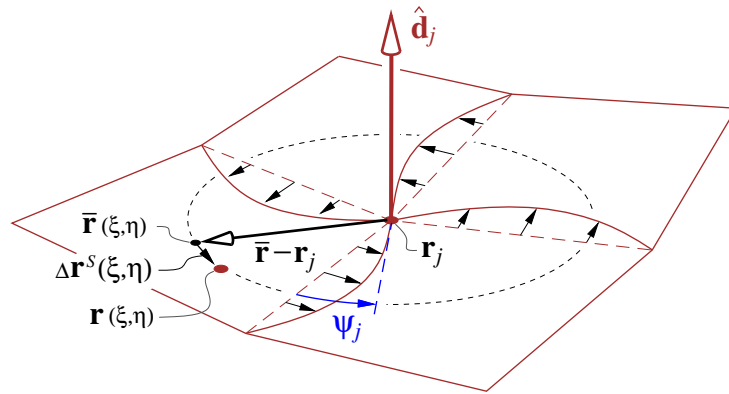


Figure 6: Displacement field of drilling angle  $\psi_j$  in the elements sharing node  $j$ .

The coefficient  $B_j$  for each edge  $j \dots j + 1$  is set explicitly such that the  $\mathbf{r}(\xi, \eta)$  surface is made orthogonal on average to the  $\hat{\mathbf{d}}_j$  vectors at the endpoints of that edge. For each edge we therefore impose the requirement

$$\hat{\mathbf{d}}_j \cdot \partial_\sigma \mathbf{r} \Big|_j - \hat{\mathbf{d}}_{j+1} \cdot \partial_\sigma \mathbf{r} \Big|_{j+1} = 0 \quad (87)$$

where the  $\sigma$  directional derivative is defined in  $\xi$ - $\eta$  parameter space along that edge, and evaluated at the endpoints as indicated. Inserting the quadratic surface form (81) into (87) and noting that

$$\hat{\mathbf{d}} \cdot \partial_\sigma \hat{\mathbf{d}} = 0, \quad \hat{\mathbf{d}}_j \cdot (\hat{\mathbf{d}}_j \times [\cdot]) = 0, \quad \check{N}_j|_j = 0, \quad \check{N}_j|_{j+1} = 0$$

and

$$\partial_\sigma \check{N}_j|_j = \frac{1}{2}, \quad \partial_\sigma \check{N}_j|_{j+1} = -\frac{1}{2}$$

then gives each edge coefficient explicitly.

$$B_j = \frac{(\hat{\mathbf{d}}_{j+1} - \hat{\mathbf{d}}_j) \cdot \partial_\sigma \bar{\mathbf{r}}}{\partial_\sigma \check{N}_j|_j - \partial_\sigma \check{N}_j|_{j+1}} = (\hat{\mathbf{d}}_{j+1} - \hat{\mathbf{d}}_j) \cdot \frac{\mathbf{r}_{j+1} - \mathbf{r}_j}{\sqrt{(\xi_{j+1} - \xi_j)^2 + (\eta_{j+1} - \eta_j)^2}} \quad (88)$$

The two higher-order surface terms in (81) have several notable and important properties:

- The higher-order formulation has the same number of primary variables per node as the underlying bilinear formulation. The result is a considerable improvement in absolute accuracy for a given resolution and computational cost compared to standard bilinear methods.
- A uniform transverse shear strain field, which will tilt all the director vectors by the same angle, will cancel in the  $\hat{\mathbf{d}}_{j+1} - \hat{\mathbf{d}}_j$  difference in equation (88). Hence, the resulting  $B_j$  coefficients will be unaffected and so the quadratic surface geometry does not depend on such a uniform transverse shear field.
- If all the nodal rotations are equal and all the directors are parallel, i.e.  $\psi_j = \psi = \text{const.}$  and  $\hat{\mathbf{d}}_j = \hat{\mathbf{d}} = \text{const.}$ , the overall term vanishes.

$$\sum_j \psi_j \hat{\mathbf{d}}_j \times (\bar{\mathbf{r}} - \mathbf{r}_j) N_j = \psi \hat{\mathbf{d}} \times \sum_j (\bar{\mathbf{r}} - \mathbf{r}_j) N_j = \psi \hat{\mathbf{d}} \times (\bar{\mathbf{r}} - \bar{\mathbf{r}}) = \mathbf{0} \quad (89)$$

A uniform-drill field on a flat element therefore gives zero membrane strains exactly.

- Both higher-order terms in (81) along an edge are defined using quantities only on that edge. Hence, this higher-order  $\mathbf{r}(\xi, \eta)$  surface representation is conformal.

### 8.3.3 Membrane and bending strain interpolation

Numerical experiments reveal that using the full  $\mathbf{a}_\alpha$  expression (82) in the strain and curvature-change definition (44) and (50) is workable but not satisfactory for distorted elements. Although the  $\mathbf{a}_\alpha$  direction is smooth and nearly continuous across element boundaries, its magnitude fluctuates about the average within each element due to the  $\hat{\mathbf{d}}$  and  $\partial_\alpha \hat{\mathbf{d}}$  terms in (86). This then produces added curvature-induced strains with spurious fluctuations over the element. These fluctuations are non-polynomial ( $\hat{\mathbf{d}}$  is rational), and therefore cannot be exactly eliminated by the Gaussian integration over the element. The approach used here is to compute all strains using the in-surface basis vectors  $\bar{\mathbf{a}}_\alpha$  which simply omit the transverse term.

$$\bar{\mathbf{a}}_\alpha \equiv \partial_\alpha \bar{\mathbf{r}} + \partial_\alpha \Delta \mathbf{r}^S \quad (90)$$

$$\check{\epsilon}_{\alpha\beta} = \frac{1}{2} (\bar{\mathbf{a}}_\alpha \cdot \bar{\mathbf{a}}_\beta - \bar{\mathbf{a}}_{0\alpha} \cdot \bar{\mathbf{a}}_{0\beta}) \quad (91)$$

$$\check{\kappa}_{\alpha\beta} = \bar{\mathbf{a}}_\alpha \cdot \partial_\beta \hat{\mathbf{d}} - \bar{\mathbf{a}}_{0\alpha} \cdot \partial_\beta \hat{\mathbf{n}}_0 \quad (92)$$

The omitted  $\partial_\alpha \Delta \mathbf{r}^N$  terms then only control the direction of the stress resultants, but not their magnitude.

### 8.3.4 Director lean interpolations

The HSM higher-order geometry representation allows the director lean (and corresponding transverse shear strain) components to be evaluated directly from definition (37) using the isoparametrically interpolated  $\hat{\mathbf{d}}$  and  $\mathbf{a}_\alpha$ , with no shear-locking problems.

Alternatively, the director lean can also be evaluated using the MITC interpolation[3], from the edge midpoints. Here, for each edge midpoint we compute

$$\check{\ell}_{\alpha_{j+1/2}} = \hat{\mathbf{d}} \cdot \partial_\alpha \bar{\mathbf{r}} \Big|_{j+1/2} \quad (93)$$

and these are then interpolated using the following standard MITC scheme to give the  $\check{\ell}_{\alpha(\xi,\eta)}$  field for a quad element.

$$\check{\ell}_1(\eta) = \frac{1}{2}(1-\eta) \check{\ell}_{1_{1/2}} - \frac{1}{2}(1+\eta) \check{\ell}_{1_{3/2}} \quad (94)$$

$$\check{\ell}_2(\xi) = \frac{1}{2}(1-\xi) \check{\ell}_{2_{4/2}} - \frac{1}{2}(1+\xi) \check{\ell}_{2_{2/2}} \quad (95)$$

The same expressions are used for interpolating  $\check{\ell}_{0\alpha}$ .

The similar MITC3 scheme is used for triangular elements[8].

### 8.3.5 Rotated nodal data

The stiffnesses of isotropic materials can be uniquely defined by the scalars  $E, \nu$  (or equivalent Lamé constants), which allows stiffness properties to be constructed locally within the element. However, the shell stiffness properties for composite materials are inherently tensor quantities which must be defined in some basis, which here is chosen to be defined by the  $\hat{\mathbf{e}}_{01}, \hat{\mathbf{e}}_{02}, \hat{\mathbf{n}}_0$  basis vectors tangent and normal to the surface. For a curved geometry these must in general differ between the nodes of an element, so the tensor stiffness data must be interpolated in some common basis. To exactly represent uniform loading and uniform strain and stress fields (and thus pass patch tests), this interpolation is typically performed in a local surface-aligned cartesian basis defined by the  $\hat{\mathbf{c}}$  vectors computed at the element centroid[9, 3] as follows.

$$\hat{\mathbf{c}}_{1\text{ref}} = \frac{\partial_\xi \mathbf{r}_0}{|\partial_\xi \mathbf{r}_0|} \Big|_{\xi_c, \eta_c}, \quad \hat{\mathbf{c}}_{n\text{ref}} = \frac{\partial_\xi \mathbf{r}_0 \times \partial_\eta \mathbf{r}_0}{|\partial_\xi \mathbf{r}_0 \times \partial_\eta \mathbf{r}_0|} \Big|_{\xi_c, \eta_c}, \quad \hat{\mathbf{c}}_{2\text{ref}} = \hat{\mathbf{c}}_{n\text{ref}} \times \hat{\mathbf{c}}_{1\text{ref}} \quad (96)$$

For an element whose undeformed shape is curved, or more precisely whose nodal  $\hat{\mathbf{n}}_0$  are not all parallel, using this basis as-is at the nodes will produce spurious cosine-error “mixing” between the tangential and normal components of the tensor node data, as suggested by the top diagram Figure 7 for the 2D case. In HSM this is avoided by using a rotated basis  $\hat{\mathbf{c}}_j$  at each node, as indicated in the bottom diagram.

The rotated vectors are obtained by the expressions

$$\delta = \hat{\mathbf{c}}_{n\text{ref}} \cdot \hat{\mathbf{n}}_{0j} \quad (97)$$

$$\boldsymbol{\alpha} = \hat{\mathbf{c}}_{n\text{ref}} \times \hat{\mathbf{n}}_{0j} \quad (98)$$

$$\hat{\mathbf{c}}_{1j} = \frac{\delta \hat{\mathbf{c}}_{1\text{ref}} + \boldsymbol{\alpha} \times \hat{\mathbf{c}}_{1\text{ref}}}{\sqrt{\delta^2 + |\boldsymbol{\alpha}|^2}} \quad (99)$$

$$\hat{\mathbf{c}}_{2j} = \frac{\delta \hat{\mathbf{c}}_{2\text{ref}} + \boldsymbol{\alpha} \times \hat{\mathbf{c}}_{2\text{ref}}}{\sqrt{\delta^2 + |\boldsymbol{\alpha}|^2}} \quad (100)$$

$$\hat{\mathbf{c}}_{nj} = \hat{\mathbf{n}}_{0j} \quad (101)$$

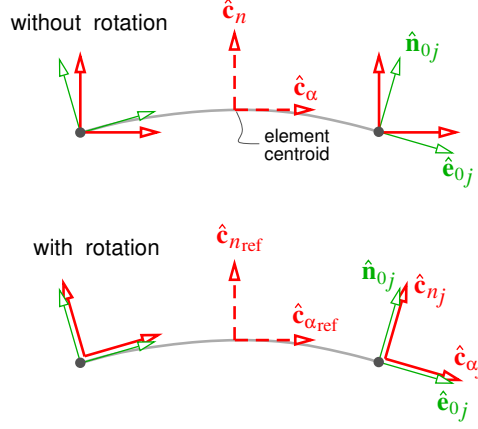


Figure 7: Rotation of 2D element cartesian  $\hat{\mathbf{c}}$  basis vectors into each node avoids spurious mixing between tangential and normal components of node tensor data.

which correspond to rotation about  $\boldsymbol{\alpha}$  through the angle  $\theta = \arctan(|\boldsymbol{\alpha}|/\delta)$ , applied to each node of the element as diagrammed in Figure 8. The components of the nodal stiffness tensors in the

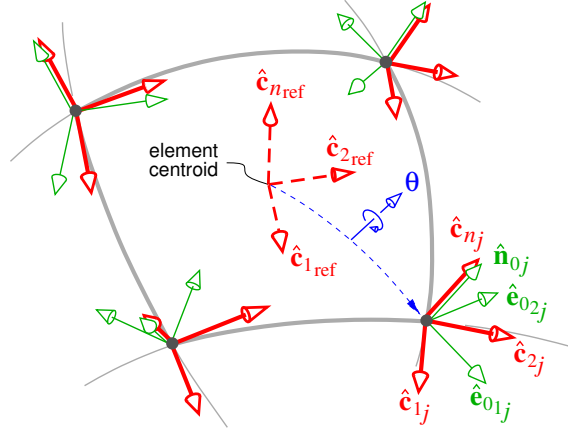


Figure 8: Cartesian  $\hat{\mathbf{c}}_{\text{ref}}$  basis vectors at element centroid of the undeformed geometry are rotated to each node  $j$  by the angle from  $\hat{\mathbf{c}}_{n\text{ref}}$  to  $\hat{\mathbf{n}}_{0j}$ . Nodal vector and tensor data is projected onto the rotated basis for interpolation over element.

rotated element cartesian basis are

$$A_{abcd}^{\hat{\mathbf{c}}} = A_{ijkl} (\hat{\mathbf{e}}_{0i} \cdot \hat{\mathbf{c}}_a) (\hat{\mathbf{e}}_{0j} \cdot \hat{\mathbf{c}}_b) (\hat{\mathbf{e}}_{0k} \cdot \hat{\mathbf{c}}_c) (\hat{\mathbf{e}}_{0\ell} \cdot \hat{\mathbf{c}}_d) \quad (102)$$

$$S_{anbn}^{\hat{\mathbf{c}}} = S_{ijn} (\hat{\mathbf{e}}_{0i} \cdot \hat{\mathbf{c}}_a) (\hat{\mathbf{e}}_{0j} \cdot \hat{\mathbf{c}}_b) \quad (103)$$

where here  $i, j, k, \ell, a, b, c, d \in \{1, 2\}$ . These projected values are then interpolated to the interior as usual.

$$A_{abcd}^{\hat{\mathbf{c}}}(\xi, \eta) = \sum_j (A_{abcd}^{\hat{\mathbf{c}}})_j N_j, \text{ etc.} \quad (104)$$

Finally, the interpolated stiffnesses are put into the local contravariant basis.

$$\check{A}^{\alpha\beta\gamma\delta} = A_{abcd}^{\hat{\mathbf{c}}} (\hat{\mathbf{c}}_a \cdot \mathbf{a}_0^\alpha) (\hat{\mathbf{c}}_b \cdot \mathbf{a}_0^\beta) (\hat{\mathbf{c}}_c \cdot \mathbf{a}_0^\gamma) (\hat{\mathbf{c}}_d \cdot \mathbf{a}_0^\delta) \quad (105)$$

$$\check{S}^{\alpha n \beta n} = S_{anbn}^{\hat{\mathbf{c}}} (\hat{\mathbf{c}}_a \cdot \mathbf{a}_0^\alpha) (\hat{\mathbf{c}}_b \cdot \mathbf{a}_0^\beta) \quad (106)$$

Note that all these projections involve only the undeformed reference configuration and do not depend on the solution, so they could be performed only once for each element and stored.

### 8.3.6 Interpolated data

The nodal data listed below is interpolated to finite-element Gauss points  $\xi_k, \eta_k$  in the element interior via the  $N_j(\xi_k, \eta_k)$  interpolation function weights. The coordinate derivatives of some data are also computed at the Gauss points.

symbol	num.	var. dep.	par. dep.	axes	description
$\mathbf{r}_0$	3		$\mathbf{r}_{0j}, \hat{\mathbf{n}}_{0j}$	$xyz$	undeformed-geometry position
$\partial_\alpha \mathbf{r}_0$	6		$\mathbf{r}_{0j}, \hat{\mathbf{n}}_{0j}$	$xyz$	undeformed-geometry position derivatives
$\hat{\mathbf{n}}_0$	3		$\hat{\mathbf{n}}_{0j}$	$xyz$	undeformed-geometry normal vector
$\partial_\alpha \hat{\mathbf{n}}_0$	6		$\hat{\mathbf{n}}_{0j}$	$xyz$	undeformed-geometry normal vector derivatives
$\mathbf{r}$	3	$\mathbf{r}_j, \hat{\mathbf{d}}_j, \psi_j$		$xyz$	deformed-geometry position
$\partial_\alpha \mathbf{r}$	6	$\mathbf{r}_j, \hat{\mathbf{d}}_j, \psi_j$		$xyz$	deformed-geometry position derivatives
$\hat{\mathbf{d}}$	3	$\hat{\mathbf{d}}_j$		$xyz$	deformed-geometry material quasi-normal vector
$\partial_\alpha \hat{\mathbf{d}}$	6	$\hat{\mathbf{d}}_j$		$xyz$	deformed-geometry material quasi-normal vector derivatives
$\mathbf{q}_{xyz}$	3		$\mathbf{q}_{xyzj}$	$xyz$	fixed-direction applied loads
$q_n$	1		$q_{nj}$	$12n$	shell-following normal applied load
$\mu$	1		$\mu_j$	—	mass/area density
$\check{A}^{\alpha\beta\gamma\delta}$	6		$\bar{\bar{A}}_j, \mathbf{r}_{0j}, \bar{\bar{\mathbf{e}}}_{0j}$	$\xi\eta$	in-surface extension stiffness matrix
$\check{B}^{\alpha\beta\gamma\delta}$	6		$\bar{\bar{B}}_j, \mathbf{r}_{0j}, \bar{\bar{\mathbf{e}}}_{0j}$	$\xi\eta$	extension/bending coupling stiffness matrix
$\check{D}^{\alpha\beta\gamma\delta}$	6		$\bar{\bar{D}}_j, \mathbf{r}_{0j}, \bar{\bar{\mathbf{e}}}_{0j}$	$\xi\eta$	bending stiffness matrix
$\check{S}^{\alpha n \beta n}$	3		$\bar{\bar{S}}_j, \mathbf{r}_{0j}, \bar{\bar{\mathbf{e}}}_{0j}$	$\xi\eta$	transverse shear compliance matrix

The interpolated geometry data is also used to compute the basis vectors and the corresponding metric and curvature tensors listed below, and computed using the expressions given in Section 6. The inverse metric tensor and contravariant basis vectors then also follow.

symbol	num.	var. dep.	par. dep.	axes	description
$\mathbf{a}_{0\alpha}$	6		$\mathbf{r}_{0j}, \hat{\mathbf{n}}_{0j}$	$xyz$	undeformed-geometry covariant basis vectors
$\check{g}_{0\alpha\beta}$	3		$\mathbf{r}_{0j}, \hat{\mathbf{n}}_{0j}$	$\xi\eta$	undeformed-geometry metric tensor
$\check{h}_{0\alpha\beta}$	3		$\mathbf{r}_{0j}, \hat{\mathbf{n}}_{0j}$	$\xi\eta$	undeformed-geometry curvature tensor
$\check{\ell}_{0\alpha}$	3		$\mathbf{r}_{0j}, \hat{\mathbf{n}}_{0j}$	$\xi\eta$	undeformed-geometry director-lean vector
$\check{g}_0$	1		$\mathbf{r}_{0j}, \hat{\mathbf{n}}_{0j}$	–	undeformed-geometry metric determinant
$\check{g}_0^{\alpha\beta}$	3		$\mathbf{r}_{0j}, \hat{\mathbf{n}}_{0j}$	$\xi\eta$	undeformed-geometry inverse metric tensor
$\mathbf{a}_0^\alpha$	6		$\mathbf{r}_{0j}, \hat{\mathbf{n}}_{0j}$	$xyz$	undeformed-geometry contravariant basis vectors
$\mathbf{a}_\alpha$	6	$\mathbf{r}_j, \hat{\mathbf{d}}_j, \psi_j$		$xyz$	deformed-geometry covariant basis vectors
$\check{g}_{\alpha\beta}$	3	$\mathbf{r}_j, \hat{\mathbf{d}}_j, \psi_j$		$\xi\eta$	deformed-geometry metric tensor
$\check{h}_{\alpha\beta}$	3	$\mathbf{r}_j, \hat{\mathbf{d}}_j, \psi_j$		$\xi\eta$	deformed-geometry curvature tensor
$\check{\ell}_\alpha$	3	$\mathbf{r}_j, \hat{\mathbf{d}}_j$		$\xi\eta$	deformed-geometry director lean vector
$\check{g}$	1	$\mathbf{r}_j, \hat{\mathbf{d}}_j, \psi_j$		–	deformed-geometry metric determinant
$\check{g}^{\alpha\beta}$	3	$\mathbf{r}_j, \hat{\mathbf{d}}_j, \psi_j$		$\xi\eta$	deformed-geometry inverse metric tensor
$\mathbf{a}^\alpha$	6	$\mathbf{r}_j, \hat{\mathbf{d}}_j, \psi_j$		$xyz$	deformed-geometry contravariant basis vectors

The curvature tensors  $\check{h}_{0\alpha\beta}$  and  $\check{h}_{\alpha\beta}$  are symmetric analytically, but not necessarily numerically. Hence, their two off-diagonal element definitions are averaged, i.e.

$$\check{h}_{21} = \check{h}_{12} := \frac{1}{2} \left( \mathbf{a}_1 \cdot \partial_2 \hat{\mathbf{d}} + \mathbf{a}_2 \cdot \partial_1 \hat{\mathbf{d}} \right) \quad (107)$$

which ensures numerical symmetry.

### 8.3.7 Strains and stresses

The metric and curvature tensors are in turn used to compute the strain and curvature-change tensors at the Gauss points.

symbol	num.	var. dep.	par. dep.	axes	description
$\check{\epsilon}_{\alpha\beta}$	3	$\mathbf{r}_j, \hat{\mathbf{d}}_j, \psi_j$	$\mathbf{r}_{0j}, \hat{\mathbf{n}}_{0j}$	$\xi\eta$	in-surface strain covariant components
$\check{\kappa}_{\alpha\beta}$	3	$\mathbf{r}_j, \hat{\mathbf{d}}_j, \psi_j$	$\mathbf{r}_{0j}, \hat{\mathbf{n}}_{0j}$	$\xi\eta$	curvature-change covariant components
$\check{\gamma}_\alpha$	2	$\mathbf{r}_j, \hat{\mathbf{d}}_j, \psi_j$	$\mathbf{r}_{0j}, \hat{\mathbf{n}}_{0j}$	$\xi\eta$	transverse shear strain covariant components

$$\check{\epsilon}_{\alpha\beta}(\xi, \eta) = \frac{1}{2} \left( \check{g}_{\alpha\beta} - \check{g}_{0\alpha\beta} \right) \quad (108)$$

$$\check{\kappa}_{\alpha\beta}(\xi, \eta) = \check{h}_{\alpha\beta} - \check{h}_{0\alpha\beta} \quad (109)$$

$$\check{\gamma}_\alpha(\xi, \eta) = \check{\ell}_\alpha - \check{\ell}_{0\alpha} \quad (110)$$

The stress and stress-moment resultants at the Gauss points are computed directly from the strain and curvature-change tensors and the interpolated stiffness matrices.

symbol	num.	var. dep.	par. dep.	axes	description
$\check{f}^{\alpha\beta}$	3	$\mathbf{r}_j, \hat{\mathbf{d}}_j, \psi_j$	$\mathbf{r}_{0j}, \hat{\mathbf{n}}_{0j}, \bar{\mathbf{e}}_{0j}, \bar{\bar{A}}_j, \bar{\bar{B}}_j$	$\xi\eta$	in-surface stress contravariant components
$\check{m}^{\alpha\beta}$	3	$\mathbf{r}_j, \hat{\mathbf{d}}_j, \psi_j$	$\mathbf{r}_{0j}, \hat{\mathbf{n}}_{0j}, \bar{\mathbf{e}}_{0j}, \bar{\bar{B}}_j, \bar{\bar{D}}_j$	$\xi\eta$	stress-moment contravariant components
$\check{f}^{\alpha n}$	2	$\mathbf{r}_j, \hat{\mathbf{d}}_j, \psi_j$	$\mathbf{r}_{0j}, \hat{\mathbf{n}}_{0j}, \bar{\mathbf{e}}_{0j}, \bar{\bar{S}}_j$	$\xi\eta$	transverse stress contravariant components

$$\check{f}^{11}_{(\xi,\eta)} = \check{A}^{11\alpha\beta} \check{\varepsilon}_{\alpha\beta} + \check{B}^{11\alpha\beta} \check{\kappa}_{\alpha\beta} \quad (111)$$

$$\check{f}^{22}_{(\xi,\eta)} = \check{A}^{22\alpha\beta} \check{\varepsilon}_{\alpha\beta} + \check{B}^{22\alpha\beta} \check{\kappa}_{\alpha\beta} \quad (112)$$

$$\check{f}^{12}_{(\xi,\eta)} = \check{A}^{12\alpha\beta} \check{\varepsilon}_{\alpha\beta} + \check{B}^{12\alpha\beta} \check{\kappa}_{\alpha\beta} \quad (113)$$

$$\check{m}^{11}_{(\xi,\eta)} = \check{B}^{11\alpha\beta} \check{\varepsilon}_{\alpha\beta} + \check{D}^{11\alpha\beta} \check{\kappa}_{\alpha\beta} \quad (114)$$

$$\check{m}^{22}_{(\xi,\eta)} = \check{B}^{22\alpha\beta} \check{\varepsilon}_{\alpha\beta} + \check{D}^{22\alpha\beta} \check{\kappa}_{\alpha\beta} \quad (115)$$

$$\check{m}^{12}_{(\xi,\eta)} = \check{B}^{12\alpha\beta} \check{\varepsilon}_{\alpha\beta} + \check{D}^{12\alpha\beta} \check{\kappa}_{\alpha\beta} \quad (116)$$

Summation over  $\alpha = 1, 2$  and  $\beta = 1, 2$  is performed as usual. For example,

$$\begin{aligned} \check{f}^{12}_{(\xi,\eta)} &= \check{A}^{1211} \check{\varepsilon}_{11} + \check{B}^{1211} \check{\kappa}_{11} \\ &+ \check{A}^{1221} \check{\varepsilon}_{21} + \check{B}^{1221} \check{\kappa}_{21} \\ &+ \check{A}^{1212} \check{\varepsilon}_{12} + \check{B}^{1212} \check{\kappa}_{12} \\ &+ \check{A}^{1222} \check{\varepsilon}_{22} + \check{B}^{1222} \check{\kappa}_{22} \end{aligned} \quad (117)$$

The transverse shear stress components are computed as follows.

$$\check{f}^{\alpha n} = \check{S}^{\alpha\beta} \check{\gamma}_{\beta} \quad (118)$$

$$\check{f}^{1n} := \check{S}^{11} \check{\gamma}_1 + \check{S}^{12} \check{\gamma}_2 \quad (119)$$

$$\check{f}^{2n} := \check{S}^{21} \check{\gamma}_1 + \check{S}^{22} \check{\gamma}_2 \quad (120)$$

### 8.3.8 Other derived data

The interpolated quantities at the Gauss points are further used to compute the secondary quantities listed below.

symbol	num.	var. dep.	par. dep.	axes	description
$\hat{\mathbf{n}}$	3	$\mathbf{r}_j, \hat{\mathbf{d}}_j$		$xyz$	normal vector
$\mathbf{q}$	3	$\mathbf{r}_j, \hat{\mathbf{d}}_j$	$\mathbf{q}_{xyzj}, q_{n_j}$	$xyz$	total applied load
$\mathbf{a}$	3	$\mathbf{r}_j, \hat{\mathbf{d}}_j, \psi_j$	$\dot{\mathbf{U}}, \dot{\mathbf{\Omega}}, \mathbf{U}, \mathbf{\Omega}$	$xyz$	acceleration

The total applied load  $\mathbf{q}$  is the sum of the fixed-direction and shell-following normal loads.

$$\mathbf{q} = \mathbf{q}_{xyz} + q_n \hat{\mathbf{n}} \quad (121)$$

For static problems (steady in the  $xyz$  frame), the local acceleration  $\mathbf{a}$  is computed as

$$\mathbf{a} = \dot{\mathbf{U}} + \mathbf{\Omega} \times \mathbf{U} + \dot{\mathbf{\Omega}} \times \mathbf{r} + \mathbf{\Omega} \times (\mathbf{\Omega} \times \mathbf{r}) \quad (122)$$

where the sum of the first two terms (equal to  $\mathbf{a}_B$  as given by (66)) is the frame linear acceleration relative to an inertial frame, the third term is the relative tangential acceleration, and the last term is the relative centripetal acceleration. Additional accelerations will appear in dynamic problems, which will be considered in a later section.

## 8.4 Equation Residuals

### 8.4.1 Residual weights and integration

HSM uses a Galerkin-type finite-element formulation, where the residual weighting function  $W_i(\xi, \eta)$  associated with node  $i$  is chosen to be the “tent” function formed from the union of the  $N_i(\xi, \eta)$  interpolants, shown in Figure 9. On each element we then have

$$W_i(\xi, \eta) = N_i(\xi, \eta) \quad (123)$$

$$\tilde{\nabla} W_i(\xi, \eta) = \tilde{\nabla} N_i(\xi, \eta) \quad (124)$$

where the weight function gradient  $\tilde{\nabla} W_i$  is defined via its element-basis components like  $\tilde{\nabla} N_i$ .

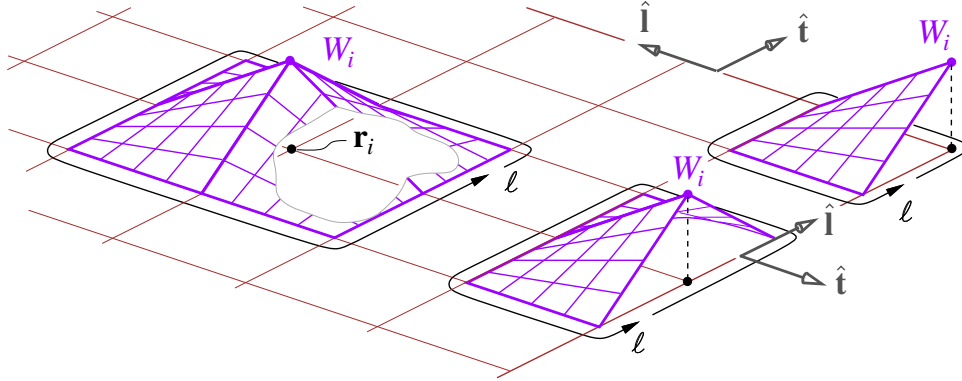


Figure 9: Residual weighting functions  $W_i(\xi, \eta)$ , variable and residual projection vectors  $\hat{\mathbf{b}}_{1_i}$ ,  $\hat{\mathbf{b}}_{2_i}(\xi, \eta)$ , and element basis vectors  $\mathbf{a}_1$ ,  $\mathbf{a}_2(\xi, \eta)$  associated with interior, edge, and corner nodes. The edge-normal and edge-parallel tangent vectors  $\hat{\mathbf{t}}$ ,  $\hat{\mathbf{l}}$  and edge length coordinate  $\ell$  are also shown.

Per standard procedure, all area integrals will be recast in terms of the element coordinates  $\xi, \eta$  and their Jacobian  $J_0$ , and then numerically evaluated using 4-point Gaussian quadrature,

$$\iint \mathcal{F} d\mathcal{A}_0 = \iint \mathcal{F} J_0 d\xi d\eta \simeq \sum_{k=1}^4 \mathcal{F}(\xi_k, \eta_k) J_0(\xi_k, \eta_k) w_k \quad (125)$$

$$J_0 = |\mathbf{a}_{0_1} \times \mathbf{a}_{0_2}| \quad (126)$$

where the index  $k$  runs over the Gauss points  $(\xi_k, \eta_k)$  and  $w_k$  are the corresponding Gauss weights. The integration is performed over the undeformed geometry, primarily because this simplifies linearization of the resulting residual expressions for Newton solution.

For the edge line integrals appearing in (32) and (33), 2-point Gaussian integration is used.

$$\int \mathcal{F} d\ell_0 = \int \mathcal{F} J_0 d\xi \simeq \sum_{k=1}^2 \mathcal{F}(\xi_k) J_0 w_k \quad (127)$$

Here,  $-1 \leq \xi \leq +1$  is the parameter along the edge, and the Jacobian is a constant  $J_0 = \Delta\ell_0/2$  where  $\Delta\ell_0$  is the edge length of the undeformed element.



### 8.4.2 Momentum residuals

The area-integral and edge-integral parts of the momentum equation (32) for node  $i$  are evaluated in the  $xyz$  axes

$$\mathcal{R}_i^f \equiv \sum_{\text{elements}} \iint \left\{ -\bar{\mathbf{f}} \cdot \tilde{\nabla} W_i + \mathbf{q} W_i + \mu (\mathbf{g} - \mathbf{a}) W_i \right\} d\mathcal{A}_0 \quad (128)$$

$$\Delta \mathcal{R}_i^f \equiv \sum_{\text{edges}} \oint \left\{ \bar{\mathbf{f}} \cdot \hat{\mathbf{t}} \right\} W_i d\ell_0 \quad (129)$$

in which the dot products are evaluated using the interpolated element-basis components as follows.

$$\begin{aligned} \bar{\mathbf{f}} \cdot \tilde{\nabla} W_i &= \left[ \check{f}^{11} \mathbf{a}_1 \mathbf{a}_1 + \check{f}^{12} \mathbf{a}_1 \mathbf{a}_2 + \check{f}^{21} \mathbf{a}_2 \mathbf{a}_1 + \check{f}^{22} \mathbf{a}_2 \mathbf{a}_2 + \check{f}^{1n} (\mathbf{a}_1 \hat{\mathbf{n}} + \hat{\mathbf{n}} \mathbf{a}_1) + \check{f}^{2n} (\mathbf{a}_2 \hat{\mathbf{n}} + \hat{\mathbf{n}} \mathbf{a}_2) \right] \\ &\quad \cdot \left[ \mathbf{a}^1 \partial_1 W_i + \mathbf{a}^2 \partial_2 W_i \right] \\ &= \left( \check{f}^{11} \partial_1 W_i + \check{f}^{12} \partial_2 W_i \right) \mathbf{a}_1 + \left( \check{f}^{21} \partial_1 W_i + \check{f}^{22} \partial_2 W_i \right) \mathbf{a}_2 + \left( \check{f}^{1n} \partial_1 W_i + \check{f}^{2n} \partial_2 W_i \right) \hat{\mathbf{n}} \end{aligned} \quad (130)$$

The dot product in (129) will be evaluated using boundary condition data, and does not need to be explicitly expanded here.

### 8.4.3 Angular momentum residuals

The area-integral and edge-integral parts of the angular momentum equation (33) for node  $i$  are evaluated in the  $xyz$  axes

$$\mathcal{R}_i^m \equiv \iint \left\{ -\hat{\mathbf{d}} \times \bar{\mathbf{m}} \cdot \tilde{\nabla} W_i + \mathbf{r} \times \left[ -\bar{\mathbf{f}} \cdot \tilde{\nabla} W_i + \mathbf{q} W_i + \mu (\mathbf{g} - \mathbf{a}) W_i \right] \right\} d\mathcal{A} = \mathbf{0} \quad (131)$$

$$\Delta \mathcal{R}_i^m \equiv \sum_{\text{edges}} \oint \left\{ \hat{\mathbf{d}} \times \bar{\mathbf{m}} \cdot \hat{\mathbf{t}} + \mathbf{r} \times \bar{\mathbf{f}} \cdot \hat{\mathbf{t}} \right\} W_i d\ell \quad (132)$$

The vectors in the  $\mathbf{r} \times [\ ]$  terms above are the force residual integrands in (128) and (129), and can be re-used here in the code implementation. The remaining term in (131) is evaluated using the interpolated element-basis components as follows.

$$\begin{aligned} \hat{\mathbf{d}} \times \bar{\mathbf{m}} \cdot \tilde{\nabla} W_i &= \hat{\mathbf{d}} \times \left[ \check{m}^{11} \mathbf{a}_1 \mathbf{a}_1 + \check{m}^{12} \mathbf{a}_1 \mathbf{a}_2 + \check{m}^{21} \mathbf{a}_2 \mathbf{a}_1 + \check{m}^{22} \mathbf{a}_2 \mathbf{a}_2 \right] \cdot \left[ \mathbf{a}^1 \partial_1 W_i + \mathbf{a}^2 \partial_2 W_i \right] \\ &= \left( \check{m}^{11} \partial_1 W_i + \check{m}^{12} \partial_2 W_i \right) \hat{\mathbf{d}} \times \mathbf{a}_1 + \left( \check{m}^{21} \partial_1 W_i + \check{m}^{22} \partial_2 W_i \right) \hat{\mathbf{d}} \times \mathbf{a}_2 \end{aligned} \quad (133)$$

## 8.5 Edge Loading Boundary Conditions

For a well-posed shell elasticity problem, two types of boundary conditions are required on all edges of the shell surface. One BC type is either on the edge force load or on the edge position, and the other BC type is either on the edge moment load or the edge-normal direction. The imposed force and moment boundary loads are Neumann-type natural BCs which are enforced weakly via the  $\Delta \mathcal{R}$  weighted-residual contributions, and will be described in this section. The imposed position and angle are Dirichlet-type BCs which in HSM are enforced strongly by replacing the overall edge node residuals with the appropriate Dirichlet constraints, and will be described in a later section. Later we will also consider internal matching conditions between two or more shells which join at an edge.

### 8.5.1 Edge interpolation

The edge loading data is interpolated from nodes to Gauss points  $\xi$  along the edge using the linear interpolation functions

$$\begin{aligned} N_1(\xi) &\equiv \frac{1}{2}(1-\xi) \\ N_2(\xi) &\equiv \frac{1}{2}(1+\xi) \\ \check{N} &\equiv \frac{1}{4}(1-\xi^2) \end{aligned} \quad (134)$$

which are the same as  $N_1$  and  $N_2$  in (71), with  $(\xi, \eta) = (\xi, -1)$ . We then have

$$\bar{\mathbf{r}}(\xi) = \sum_{j=1}^2 \mathbf{r}_j N_j \quad (135)$$

$$\mathbf{d}(\xi) = \sum_{j=1}^2 \hat{\mathbf{d}}_j N_j \quad (136)$$

$$\hat{\mathbf{d}}(\xi) = \frac{\mathbf{d}}{|\mathbf{d}|} \quad (137)$$

To exactly match the higher-order element-interior geometry, the edge geometry here also includes the curvature and drilling rotation angle terms.

$$\mathbf{r}(\xi) = \bar{\mathbf{r}}(\xi) + \hat{\mathbf{d}}(\xi) B \check{N}(\xi) + \sum_{j=1}^2 \psi_j \hat{\mathbf{d}}_j \times (\bar{\mathbf{r}}(\xi) - \mathbf{r}_j) N_j(\xi) \quad (138)$$

$$\begin{aligned} \mathbf{a}_1(\xi) &= \partial_\xi \mathbf{r} \\ &= \partial_\xi \bar{\mathbf{r}} + B \left( \partial_\xi \hat{\mathbf{d}} \check{N} + \hat{\mathbf{d}} \partial_\xi \check{N} \right) + \sum_{j=1}^2 \psi_j \hat{\mathbf{d}}_j \times [\partial_\xi \bar{\mathbf{r}} N_j + (\bar{\mathbf{r}} - \mathbf{r}_j) \partial_\xi N_j] \end{aligned} \quad (139)$$

The edge curvature coefficient is defined the same way as for element-interior interpolation.

$$B = (\hat{\mathbf{d}}_2 - \hat{\mathbf{d}}_1) \cdot \frac{\mathbf{r}_2 - \mathbf{r}_1}{\xi_2 - \xi_1} \quad (140)$$

### 8.5.2 Loading boundary condition axes

Imposed-load boundary conditions are specified either along the global  $xyz$  axes, or alternatively along the *edge axes*  $tld$  which are defined by the edge basis vectors  $\hat{\mathbf{t}}, \hat{\mathbf{l}}, \hat{\mathbf{d}}$ .

The local material quasi-normal vector  $\hat{\mathbf{d}}$  is obtained via spherical interpolation from the edge nodes, as described above. The edge-parallel vector  $\hat{\mathbf{l}}$  is defined to lie along the interpolated surface, and the edge-normal vector  $\hat{\mathbf{t}}$  tangent to the surface is their cross product.

$$\hat{\mathbf{l}}(\xi) = \mathbf{a}_1 / |\mathbf{a}_1| \quad (141)$$

$$\hat{\mathbf{t}}(\xi) = \hat{\mathbf{l}} \times \hat{\mathbf{d}} \quad (142)$$

The table below lists all the solution variable quantities interpolated along the edge which are needed to construct the boundary conditions. The  $\hat{\mathbf{l}}_0, \hat{\mathbf{t}}_0$  vectors are needed only for edge-joining

conditions.

symbol	num.	var. dep.	par. dep.	axes	description
$\mathbf{r}_0$	3		$\mathbf{r}_{0j}, \hat{\mathbf{n}}_{0j}$	$xyz$	undeformed-geometry position
$\partial_\alpha \mathbf{r}_0$	6		$\mathbf{r}_{0j}, \hat{\mathbf{n}}_{0j}$	$xyz$	undeformed-geometry position derivatives
$\hat{\mathbf{n}}_0$	3		$\hat{\mathbf{n}}_{0j}$	$xyz$	undeformed-geometry normal vector
$\hat{\mathbf{l}}_0$	3		$\mathbf{r}_{0j}, \hat{\mathbf{n}}_{0j}$	$xyz$	undeformed-geometry edge-parallel unit vector
$\hat{\mathbf{t}}_0$	3		$\mathbf{r}_{0j}, \hat{\mathbf{n}}_{0j}$	$xyz$	undeformed-geometry edge-normal unit vector
$\mathbf{r}$	3	$\mathbf{r}_j, \hat{\mathbf{d}}_j, \psi_j$		$xyz$	deformed-geometry position
$\partial_\alpha \mathbf{r}$	6	$\mathbf{r}_j, \hat{\mathbf{d}}_j, \psi_j$		$xyz$	deformed-geometry position derivatives
$\hat{\mathbf{d}}$	3	$\hat{\mathbf{d}}_j$		$xyz$	deformed-geometry material quasi-normal vector
$\hat{\mathbf{l}}$	3	$\mathbf{r}_j, \hat{\mathbf{d}}_j, \psi_j$		$xyz$	deformed-geometry edge-parallel unit vector
$\hat{\mathbf{t}}$	3	$\mathbf{r}_j, \hat{\mathbf{d}}_j, \psi_j$		$xyz$	deformed-geometry edge-normal unit vector

### 8.5.3 Edge loading boundary condition data

All the boundary condition data which can be imposed on the shell edges is listed in the table below. For generality we specify and superimpose two separate loads: fixed-direction loads in the  $xyz$  axes, and shell-following loads in the  $tld$  axes, in the same manner as the overall surface load  $\mathbf{q}$  was obtained from  $\mathbf{q}_{xyz}$  and  $q_n$ . All these quantities are interpolated along the edge to the Gauss points.

symbol	num.	axes	description
$\mathbf{f}_{xyzBC_j}$	3	$xyz$	imposed fixed-direction edge boundary force/length
$f_{tBC_j}$	1	$tld$	imposed shell-following edge boundary $t$ -force/length
$f_{\ell BC_j}$	1	$tld$	imposed shell-following edge boundary $\ell$ -force/length
$f_{dBC_j}$	1	$tld$	imposed shell-following edge boundary $d$ -force/length
$\mathbf{m}_{xyzBC_j}$	3	$xyz$	imposed fixed-direction edge boundary moment/length
$m_{tBC_j}$	1	$tld$	imposed shell-following edge boundary bending moment/length
$m_{\ell BC_j}$	1	$tld$	imposed shell-following edge boundary torsion moment/length
$m_{dBC_j}$	1	$tld$	imposed shell-following edge boundary drilling moment/length

The specified edge force/length and moment/length over each boundary edge segment are constructed as

$$(\bar{\mathbf{f}} \cdot \hat{\mathbf{t}})_{BC} \equiv \mathbf{f}_{BC}(\xi) = \mathbf{f}_{xyzBC} + f_{tBC} \hat{\mathbf{t}} + f_{\ell BC} \hat{\mathbf{l}} + f_{dBC} \hat{\mathbf{d}} \quad (143)$$

$$(\hat{\mathbf{d}} \times \bar{\mathbf{m}} \cdot \hat{\mathbf{t}})_{BC} \equiv \mathbf{m}_{BC}(\xi) = \mathbf{m}_{xyzBC} + m_{tBC} \hat{\mathbf{t}} + m_{\ell BC} \hat{\mathbf{l}} + m_{dBC} \hat{\mathbf{d}} \quad (144)$$

which are then used in the edge-integral residual contributions (129) and (132).

$$\Delta \mathcal{R}_i^f \equiv \sum_{\text{edges}} \int \mathbf{f}_{BC} W_i d\ell_0 \quad (145)$$

$$\Delta \mathcal{R}_i^m \equiv \sum_{\text{edges}} \int (\mathbf{m}_{BC} + \mathbf{r} \times \mathbf{f}_{BC}) W_i d\ell_0 \quad (146)$$

## 8.6 Variable and Residual Projection Vectors

### 8.6.1 Projection vector definitions

To minimize the number of unknowns, and to enable the imposition of strong (Dirichlet) boundary conditions, we define local *projection basis vectors*  $\hat{\mathbf{b}}_{1_i}$ ,  $\hat{\mathbf{b}}_{2_i}$ ,  $\hat{\mathbf{b}}_{n_i}$  at each discrete node  $i$ . It is desirable that these vectors are orthogonal, which will then minimize the coupling between the projected equations, but this is not required.

For all nodes, we define

$$\hat{\mathbf{b}}_{n_i} = \hat{\mathbf{d}}_i \quad (147)$$

and then define the remaining two vectors depending on where node  $i$  lies.

**Interior and Neumann BC nodes.** For interior nodes, and edge nodes which have only loading boundary conditions,  $\hat{\mathbf{b}}_{1_i}$  and  $\hat{\mathbf{b}}_{2_i}$  are arbitrary as long as they span the shell reference surface. A simple and numerically stable procedure is to choose  $\hat{\mathbf{b}}_{1_i}$  to be the unit vector which is along the smallest component of  $\hat{\mathbf{d}}_i = d_{x_i} \hat{\mathbf{x}} + d_{y_i} \hat{\mathbf{y}} + d_{z_i} \hat{\mathbf{z}}$ , and orthogonalize it against  $\hat{\mathbf{d}}_i$ . Specifically, we compute

$$\text{if } |d_{x_i}| \leq \min(|d_{y_i}|, |d_{z_i}|) : \mathbf{b}_1 = \hat{\mathbf{x}} - \hat{\mathbf{d}}_i (\hat{\mathbf{d}}_i \cdot \hat{\mathbf{x}}) = \left\{ 1 - d_{x_i}^2, -d_{y_i} d_{x_i}, -d_{z_i} d_{x_i} \right\}^T \quad (148)$$

$$\text{if } |d_{y_i}| \leq \min(|d_{x_i}|, |d_{z_i}|) : \mathbf{b}_1 = \hat{\mathbf{y}} - \hat{\mathbf{d}}_i (\hat{\mathbf{d}}_i \cdot \hat{\mathbf{y}}) = \left\{ -d_{x_i} d_{y_i}, 1 - d_{y_i}^2, -d_{z_i} d_{y_i} \right\}^T \quad (149)$$

$$\text{if } |d_{z_i}| \leq \min(|d_{x_i}|, |d_{y_i}|) : \mathbf{b}_1 = \hat{\mathbf{z}} - \hat{\mathbf{d}}_i (\hat{\mathbf{d}}_i \cdot \hat{\mathbf{z}}) = \left\{ -d_{x_i} d_{z_i}, -d_{y_i} d_{z_i}, 1 - d_{z_i}^2 \right\}^T \quad (150)$$

which is then normalized to get  $\hat{\mathbf{b}}_{1_i}$ .

$$\hat{\mathbf{b}}_{1_i} = \mathbf{b}_1 / |\mathbf{b}_1| \quad (151)$$

We then set  $\hat{\mathbf{b}}_{2_i}$  perpendicular to both  $\hat{\mathbf{d}}_i$  and  $\hat{\mathbf{b}}_{1_i}$ .

$$\hat{\mathbf{b}}_{2_i} = \hat{\mathbf{d}}_i \times \hat{\mathbf{b}}_{1_i} \quad (152)$$

**Boundary nodes with one constraint plane.** Some boundary nodes have Dirichlet boundary conditions which have one *constraint plane* on which the node position  $\mathbf{r}_i$  is constrained to lie, or on which the material quasi-normal vector  $\hat{\mathbf{d}}_i$  is constrained to lie, or both. An example is a node on a symmetry plane, or a pinned or clamped point which is free to translate within a plane tangent to the surface. For such nodes we define  $\hat{\mathbf{b}}_{1_i}$  to be normal vector of that plane,

$$\hat{\mathbf{b}}_{1_i} = \frac{\mathbf{n}_{BC_i}}{|\mathbf{n}_{BC_i}|} \quad (153)$$

and then define

$$\hat{\mathbf{b}}_{2_i} = \hat{\mathbf{d}}_i \times \hat{\mathbf{b}}_{1_i} \quad (154)$$

**Boundary nodes with two constraint planes.** Some boundary nodes have Dirichlet boundary conditions which have two constraint planes, so that the node  $\mathbf{r}_i$  location and  $\hat{\mathbf{d}}_i$  vector must lie on the line formed by their intersection. An example is the corner node at the intersection of two symmetry planes. In this case,  $\hat{\mathbf{b}}_{1_i}$  and  $\hat{\mathbf{b}}_{2_i}$  are specified to be the two normal vectors of the two planes.

$$\hat{\mathbf{b}}_{1_i} = \frac{\mathbf{n}_{BC_i}^{(1)}}{|\mathbf{n}_{BC_i}^{(1)}|} \quad (155)$$

$$\hat{\mathbf{b}}_{2_i} = \frac{\mathbf{n}_{BC_i}^{(2)}}{|\mathbf{n}_{BC_i}^{(2)}|} \quad (156)$$

### 8.6.2 Variable projection

The projection vectors are used to define perturbations of the primary vector variables,

$$\delta \mathbf{r}_i = \hat{\mathbf{b}}_{1_i} \delta r_{1_i} + \hat{\mathbf{b}}_{2_i} \delta r_{2_i} + \hat{\mathbf{b}}_{n_i} \delta r_{n_i} \quad (157)$$

$$\delta \hat{\mathbf{d}}_i = \hat{\mathbf{b}}_{1_i} \delta d_{1_i} + \hat{\mathbf{b}}_{2_i} \delta d_{2_i} + \hat{\mathbf{b}}_{n_i} \delta d_{n_i} \quad (158)$$

which can represent either the linearized variables in a perturbation analysis, or the variable changes in a Newton iteration solution procedure.

Since  $\hat{\mathbf{d}}_i$  is defined to be a unit vector, one of the required equation residuals for node  $i$  is

$$\mathcal{R}_i(\hat{\mathbf{d}}_i) \equiv \hat{\mathbf{d}}_i \cdot \hat{\mathbf{d}}_i - 1 = 0 \quad (159)$$

which has the following linearized form in the Newton iteration system.

$$\delta \mathcal{R}_i = -\mathcal{R}_i \quad (160)$$

$$2 \hat{\mathbf{d}}_i \cdot \delta \hat{\mathbf{d}}_i = 1 - \hat{\mathbf{d}}_i \cdot \hat{\mathbf{d}}_i \quad (161)$$

Substituting for  $\delta \hat{\mathbf{d}}_i$  using the projection (158), and assuming  $|\hat{\mathbf{d}}_i| = 1$ , gives

$$\delta d_{n_i} = 0 \quad (162)$$

so that the  $\delta d_{n_i}$  variables are known to be zero a priori. These can therefore be omitted from the Newton system, thus reducing the number of Newton change variables from 7 to 6, i.e. from  $(\delta \mathbf{r}, \delta \hat{\mathbf{d}}, \delta \psi)_i$  to  $(\delta r_1, \delta r_2, \delta r_n, \delta d_1, \delta d_2, \delta \psi)_i$ .

Like the Newton variables, the vector residuals will also be projected onto the perturbation basis vectors. The main purpose here is to minimize the coupling between the equation components and maximize the diagonal dominance of the overall Jacobian matrix, which will in general improve an iterative solution method of the Newton linear system. So for example, the  $\hat{\mathbf{b}}_1$  component of the force equilibrium equation at a node will predominantly govern  $\delta r_1$  at that node, and the other related variables  $\delta r_2, \delta r_n, \delta \psi$ , etc. will have a much weaker influence.

A necessary precaution during solution iteration is that each  $\hat{\mathbf{d}}_i$  must maintain its unit magnitude, to make residual (159) always zero and thus allow  $\delta d_{n_i}$  to be dropped in the next iteration. This is ensured by rescaling each  $\hat{\mathbf{d}}_i$  to unit magnitude after its Newton update, as follows.

$$\mathbf{d}_i = \hat{\mathbf{d}}_i + \hat{\mathbf{b}}_{1_i} \delta d_{1_i} + \hat{\mathbf{b}}_{2_i} \delta d_{2_i} \quad (163)$$

$$\hat{\mathbf{d}}_i = \frac{\mathbf{d}_i}{|\mathbf{d}_i|} \quad (164)$$

The magnitude change due to this rescaling is  $\mathcal{O}\{\delta^2\}$ , so that it does not degrade the quadratic convergence of the Newton iteration sequence.

### 8.6.3 Residual projection

The vector residuals, including any loading BC contributions, are also projected onto the  $\hat{\mathbf{b}}_{1_i}, \hat{\mathbf{b}}_{2_i}, \hat{\mathbf{b}}_{n_i}$  vectors of the corresponding node.

$$\begin{Bmatrix} \mathcal{R}_i^{f_1} \\ \mathcal{R}_i^{f_2} \\ \mathcal{R}_i^{f_n} \end{Bmatrix} \equiv \begin{bmatrix} - & \hat{\mathbf{b}}_{1_i} & - \\ - & \hat{\mathbf{b}}_{2_i} & - \\ - & \hat{\mathbf{b}}_{n_i} & - \end{bmatrix} \cdot \begin{Bmatrix} | \\ \mathcal{R}_i^f + \Delta \mathcal{R}_i^f \\ | \end{Bmatrix} \quad (165)$$

$$\begin{Bmatrix} \mathcal{R}_i^{m_1} \\ \mathcal{R}_i^{m_2} \\ \mathcal{R}_i^{m_n} \end{Bmatrix} \equiv \begin{bmatrix} - & \hat{\mathbf{b}}_{2_i} & - \\ - & \hat{\mathbf{b}}_{1_i} & - \\ - & \hat{\mathbf{b}}_{n_i} & - \end{bmatrix} \cdot \begin{Bmatrix} | \\ \mathcal{R}_i^m + \Delta \mathcal{R}_i^m \\ | \end{Bmatrix} \quad (166)$$

Note that in (166), projection onto  $\hat{\mathbf{b}}_2$  defines  $\mathcal{R}^{m_1}$ , and projection onto  $\hat{\mathbf{b}}_1$  defines  $\mathcal{R}^{m_2}$ , which makes  $\mathcal{R}^{m_1}$  and  $\mathcal{R}^{m_2}$  the primary constraints on  $\delta d_1$  and  $\delta d_2$ , respectively. This makes the resulting Jacobian matrix diagonally dominant, and enables the substitution of the most appropriate residual rows with strong boundary conditions, as described next.

## 8.7 Geometry Boundary Conditions

Position or angle boundary conditions are of the Dirichlet type, and are imposed by replacing the appropriate natural residuals with the Dirichlet constraint residuals.

### 8.7.1 Dirichlet boundary condition data

All the boundary condition data which can be imposed on any shell node is listed in the table below. The node position is specified by  $\mathbf{r}_{\text{BC}}$  which is arbitrary, although in most cases it will be the same as  $\mathbf{r}_0$  of the undeformed geometry. The position can be fixed in either all three directions, or optionally forced to lie in only two planes, or only one planes. The latter partial-restraint cases are specified by the restraint-plane  $\mathbf{n}_{\text{BC}}$  normal vectors. The director orientation is specified via the  $\mathbf{t}_{\text{BC}}$  vectors, which define either one or two planes in which the director is forced to lie.

For imposing symmetry-plane boundary conditions, the symmetry plane is specified by one point  $\mathbf{r}_{\text{SP}}$  on the plane, and a vector  $\mathbf{n}_{\text{SP}}$  normal to the plane. Another point and normal vector is specified at a double-symmetry plane.

symbol	num.	axes	description
$\mathbf{r}_{\text{BC}j}$	3	$xyz$	imposed edge boundary position (also used as $\mathbf{r}_{\text{SP}}$ )
$\mathbf{n}_{\text{BC}j}^{(1)}$	3	$xyz$	$\mathbf{r}$ -restraint plane 1 normal vector (also used as $\mathbf{n}_{\text{SP}}$ )
$\mathbf{n}_{\text{BC}j}^{(2)}$	3	$xyz$	$\mathbf{r}$ -restraint plane 2 normal vector
$\mathbf{t}_{\text{BC}j}^{(1)}$	3	$xyz$	$\hat{\mathbf{d}}$ -restraint plane 1 normal vector
$\mathbf{t}_{\text{BC}j}^{(2)}$	3	$xyz$	$\hat{\mathbf{d}}$ -restraint plane 2 normal vector

### 8.7.2 Target equations for Dirichlet boundary conditions

After the residual and variable projections onto  $\hat{\mathbf{b}}_1, \hat{\mathbf{b}}_2, \hat{\mathbf{b}}_n$  are applied, each variable is predominantly governed by a Poisson type equation. To impose a Dirichlet BC on any variable in a well-posed manner, the Dirichlet BC residual must replace the corresponding Poisson residual for that variable, as listed in the table below.

$$\begin{aligned}
\mathcal{R}^{f_1} &\sim \tilde{\nabla}^2 r_1 &\rightarrow \mathcal{R}^{r_1} &\sim r_1 \\
\mathcal{R}^{f_2} &\sim \tilde{\nabla}^2 r_2 &\rightarrow \mathcal{R}^{r_2} &\sim r_2 \\
\mathcal{R}^{f_n} &\sim \tilde{\nabla}^2 r_n &\rightarrow \mathcal{R}^{r_n} &\sim r_n \\
\mathcal{R}^{m_1} &\sim \tilde{\nabla}^2 d_1 &\rightarrow \mathcal{R}^{d_1} &\sim d_1 \\
\mathcal{R}^{m_2} &\sim \tilde{\nabla}^2 d_2 &\rightarrow \mathcal{R}^{d_2} &\sim d_2 \\
\mathcal{R}^{m_n} &\sim \tilde{\nabla}^2 \psi &\rightarrow \mathcal{R}^\psi &\sim \psi
\end{aligned}$$

Specifically,  $\mathcal{R}^{r_1}$  must replace  $\mathcal{R}^{f_1}$ ,  $\mathcal{R}^{r_2}$  must replace  $\mathcal{R}^{f_2}$ , etc.

**Node displacement.** The specified position of node  $i$  is imposed by replacing the two in-surface force equilibrium residuals and the single compatibility residual with the following three position-constraint residuals  $\mathcal{R}_i^r$ .

$$\begin{Bmatrix} \mathcal{R}_i^{f_1} \\ \mathcal{R}_i^{f_2} \\ \mathcal{R}_i^{f_n} \end{Bmatrix} \leftarrow \begin{Bmatrix} \mathcal{R}_i^{r_1} \\ \mathcal{R}_i^{r_2} \\ \mathcal{R}_i^{r_n} \end{Bmatrix} \equiv \begin{bmatrix} - & \hat{\mathbf{b}}_{1_i} & - \\ - & \hat{\mathbf{b}}_{2_i} & - \\ - & \hat{\mathbf{b}}_{n_i} & - \end{bmatrix} \cdot \begin{Bmatrix} | \\ \mathbf{r}_i - \mathbf{r}_{\text{BC}_i} \\ | \end{Bmatrix} \quad (167)$$

Either one or two or three of these residuals can be imposed, as dictated by the number of restrained degrees of freedom in the physical boundary condition.

**Node director direction.** The shell surface orientation at any node can be imposed by requiring the shell material quasi-normal vector to lie within the specified sliding plane defined by either the  $\hat{\mathbf{b}}_1$  or  $\hat{\mathbf{b}}_2$  vector, and typically the drilling rotation is also restrained at such points. The corresponding residuals replace the in-surface moment equilibrium equations.

$$\begin{Bmatrix} \mathcal{R}_i^{m_1} \\ \mathcal{R}_i^{m_2} \end{Bmatrix} \leftarrow \begin{Bmatrix} \mathcal{R}_i^{d_1} \\ \mathcal{R}_i^{d_2} \end{Bmatrix} \equiv \begin{bmatrix} - & \hat{\mathbf{b}}_{1_i} & - \\ - & \hat{\mathbf{b}}_{2_i} & - \end{bmatrix} \cdot \begin{Bmatrix} | \\ \hat{\mathbf{d}}_i \\ | \end{Bmatrix} \quad (168)$$

Either one or two of these residuals can be imposed, as dictated by the physical boundary condition. A clamped edge or a single symmetry plane edge would have only the  $\mathcal{R}_i^{m_1}$  replaced with  $\mathcal{R}_i^{d_1}$ . A double symmetry plane edge would have both residuals replaced, thus completely specifying the  $\hat{\mathbf{d}}_i$  vector at that node.

**Drilling constraint.** For a well-posed problem, a Dirichlet BC on the drilling angle must be specified for at least one point, typically wherever either  $\mathbf{r}$  and/or  $\hat{\mathbf{d}}$  are also specified. This constraint replaces the normal moment equation.

$$\mathcal{R}_i^{m_n} \leftarrow \mathcal{R}_i^\psi \equiv \psi_i \quad (169)$$

## 8.8 Node Joining Conditions

The present HSM allows a shell to be built up of multiple pieces which are joined at nodes. Assuming the joint is rigid, we must enforce matching conditions on the primary variables at adjacent nodes

$()$  and  $()'$  on the two shell pieces. For this we first define joint basis vectors and the joint angle  $\vartheta_J$ ,

$$\boldsymbol{\alpha} = \hat{\mathbf{d}}_i \times \hat{\mathbf{d}}_{i'} \quad (170)$$

$$\boldsymbol{\beta} = \hat{\mathbf{d}}_i + \hat{\mathbf{d}}_{i'} \quad (171)$$

$$\boldsymbol{\gamma} = \hat{\mathbf{d}}_i - \hat{\mathbf{d}}_{i'} \quad (172)$$

$$\hat{\mathbf{l}}_J = \begin{cases} \hat{\mathbf{b}}_{1_i} & , \quad |\boldsymbol{\alpha}| < 10^{-6} \\ \boldsymbol{\alpha}/|\boldsymbol{\alpha}| & , \quad |\boldsymbol{\alpha}| \geq 10^{-6} \end{cases} \quad (173)$$

$$\hat{\mathbf{n}}_J = \begin{cases} \boldsymbol{\beta}/|\boldsymbol{\beta}| & , \quad |\boldsymbol{\beta}| > |\boldsymbol{\gamma}| \\ \boldsymbol{\gamma}/|\boldsymbol{\gamma}| & , \quad |\boldsymbol{\gamma}| \geq |\boldsymbol{\beta}| \end{cases} \quad (174)$$

$$\hat{\mathbf{t}}_J = \hat{\mathbf{l}}_J \times \hat{\mathbf{n}}_J \quad (175)$$

$$\vartheta_J = \text{atan2}(\boldsymbol{\alpha} \cdot \hat{\mathbf{l}}_J, \hat{\mathbf{d}}_i \cdot \hat{\mathbf{d}}_{i'}) \quad (176)$$

where  $\hat{\mathbf{l}}_J$  is normal to the plane containing both  $\hat{\mathbf{d}}_i$  and  $\hat{\mathbf{d}}_{i'}$ ,  $\hat{\mathbf{n}}_J$  bisects the smaller angle between the lines containing  $\hat{\mathbf{d}}_i$  and  $\hat{\mathbf{d}}_{i'}$ , and  $\hat{\mathbf{t}}_J$  bisects the larger angle, as sketched in Figure 10.

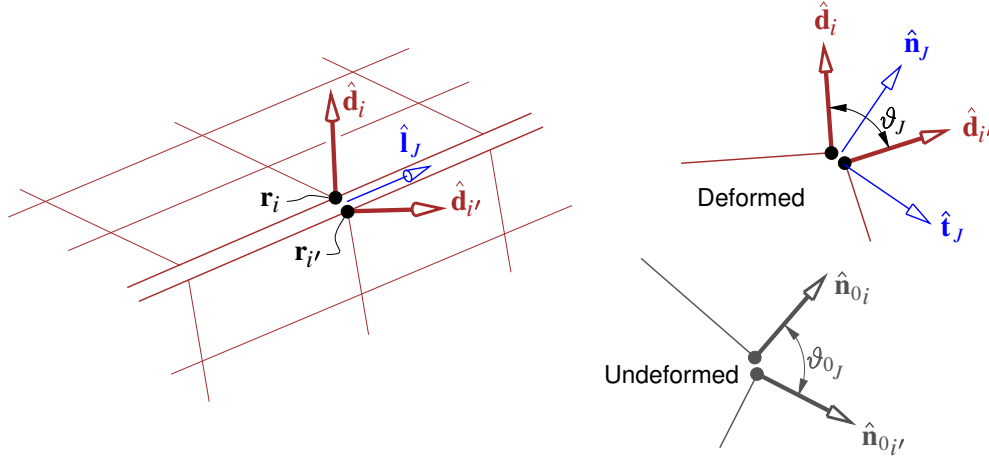


Figure 10: Vectors and angles involved in joint matching equations.

### 8.8.1 Force and position matching

The physical force matching condition at the edge is that the an infinitesimal strip of material along the edge is force-free. This is imposed by adding the cartesian force residuals of the two adjacent nodes, and then projecting as usual onto the vectors of node  $i$ .

$$\begin{Bmatrix} \mathcal{R}_i^{f1} \\ \mathcal{R}_i^{f2} \\ \mathcal{R}_i^{fn} \end{Bmatrix} \leftarrow \begin{Bmatrix} \mathcal{R}_i^{\Sigma f1} \\ \mathcal{R}_i^{\Sigma f2} \\ \mathcal{R}_i^{\Sigma fn} \end{Bmatrix} \equiv \begin{bmatrix} - & \hat{\mathbf{b}}_{1_i} & - \\ - & \hat{\mathbf{b}}_{2_i} & - \\ - & \hat{\mathbf{b}}_{n_i} & - \end{bmatrix} \cdot \begin{Bmatrix} | \\ \mathcal{R}_i^f + \mathcal{R}_{i'}^f \\ | \end{Bmatrix} \quad (177)$$

In the code implementation, the summed force residuals replace those for node  $i$  as indicated. The force residuals for node  $i'$  are then cleared and replaced with position continuity residuals on the node coordinates. These have the same form as the specified-position constraints (167).

$$\begin{Bmatrix} \mathcal{R}_{i'}^{f1} \\ \mathcal{R}_{i'}^{f2} \\ \mathcal{R}_{i'}^{fn} \end{Bmatrix} \leftarrow \begin{Bmatrix} \mathcal{R}_{i'}^{\Delta r1} \\ \mathcal{R}_{i'}^{\Delta r2} \\ \mathcal{R}_{i'}^{\Delta rn} \end{Bmatrix} \equiv \begin{bmatrix} - & \hat{\mathbf{b}}_{1_{i'}} & - \\ - & \hat{\mathbf{b}}_{2_{i'}} & - \\ - & \hat{\mathbf{b}}_{n_{i'}} & - \end{bmatrix} \cdot \begin{Bmatrix} | \\ \mathbf{r}_i - \mathbf{r}_{i'} \\ | \end{Bmatrix} \quad (178)$$



### 8.8.2 Moment and angle matching

The physical moment matching condition at the edge is that the an infinitesimal strip of material along the edge is moment-free. This is imposed by adding the cartesian moment residuals of the two adjacent nodes, and then projecting as usual onto the vectors of node  $i$ .

$$\begin{Bmatrix} \mathcal{R}_i^{m_1} \\ \mathcal{R}_i^{m_2} \\ \mathcal{R}_i^{m_n} \end{Bmatrix} \leftarrow \begin{Bmatrix} \mathcal{R}_i^{\Sigma m_1} \\ \mathcal{R}_i^{\Sigma m_2} \\ \mathcal{R}_i^{\Sigma m_n} \end{Bmatrix} \equiv \begin{bmatrix} - & \hat{\mathbf{b}}_{1_i} & - \\ - & \hat{\mathbf{b}}_{2_i} & - \\ - & \hat{\mathbf{b}}_{n_i} & - \end{bmatrix} \cdot \begin{Bmatrix} | \\ \mathcal{R}_i^m + \mathcal{R}_{i'}^m \\ | \end{Bmatrix} \quad (179)$$

The summed moment residuals replace those of node  $i$  as indicated. The moment residuals for node  $i'$  are then cleared and replaced with constraints which force  $\hat{\mathbf{d}}_i$  and  $\hat{\mathbf{d}}_{i'}$  to move as a rigid body. Consider an arbitrary material line element  $\mathbf{s}_i$  attached at one end to node  $\mathbf{r}_i$ . The change in this element due to the changes  $\delta d_{1_i}, \delta d_{2_i}, \delta \psi_i$  will be

$$\delta \mathbf{s}_i = \left( \hat{\mathbf{b}}_{1_i} \delta d_{1_i} + \hat{\mathbf{b}}_{2_i} \delta d_{2_i} + \hat{\mathbf{d}}_i \delta \psi_i \right) \times \mathbf{s}_i \quad (180)$$

and likewise for node  $i'$ . The requirement that nodes  $i$  and  $i'$  rotate as a rigid body then given by  $\delta \mathbf{s}_i - \delta \mathbf{s}_{i'} = \mathbf{0}$ , which we project onto the  $\hat{\mathbf{t}}_J$  and  $\hat{\mathbf{n}}_J$  joint vectors. In lieu of projecting onto the remaining  $\hat{\mathbf{l}}_J$  vector, we instead require  $\vartheta_J$  to be equal to its undeformed-geometry value  $\vartheta_{0_J}$  (see Figure 10), so that this angle match will be exact at convergence regardless of geometric nonlinearities introduced by large initial updates.

$$\begin{bmatrix} - & \hat{\mathbf{t}}_J & - \\ - & \hat{\mathbf{n}}_J & - \end{bmatrix} \cdot \begin{Bmatrix} | \\ \delta \mathbf{s}_i - \delta \mathbf{s}_{i'} \\ | \end{Bmatrix} = \begin{Bmatrix} 0 \\ 0 \end{Bmatrix} \quad (181)$$

$$\mathcal{R}^\vartheta \equiv \vartheta_J - \vartheta_{0_J} \quad (182)$$

The linearized  $\mathcal{R}_{i'}^m$  residual equations are then replaced by

$$\begin{aligned} & \begin{bmatrix} \hat{\mathbf{t}}_J \cdot \hat{\mathbf{b}}_{1_i} & \hat{\mathbf{t}}_J \cdot \hat{\mathbf{b}}_{2_i} & \hat{\mathbf{t}}_J \cdot \hat{\mathbf{d}}_i \\ \hat{\mathbf{n}}_J \cdot \hat{\mathbf{b}}_{1_i} & \hat{\mathbf{n}}_J \cdot \hat{\mathbf{b}}_{2_i} & \hat{\mathbf{n}}_J \cdot \hat{\mathbf{d}}_i \\ \partial \mathcal{R}^\vartheta / \partial \hat{\mathbf{d}}_i \cdot \hat{\mathbf{b}}_{1_i} & \partial \mathcal{R}^\vartheta / \partial \hat{\mathbf{d}}_i \cdot \hat{\mathbf{b}}_{2_i} & \partial \mathcal{R}^\vartheta / \partial \hat{\mathbf{d}}_i \cdot \hat{\mathbf{d}}_i \end{bmatrix} \begin{Bmatrix} \delta d_1 \\ \delta d_2 \\ \delta \psi \end{Bmatrix}_i \\ & - \begin{bmatrix} \hat{\mathbf{t}}_J \cdot \hat{\mathbf{b}}_{1_i} & \hat{\mathbf{t}}_J \cdot \hat{\mathbf{b}}_{2_i} & \hat{\mathbf{t}}_J \cdot \hat{\mathbf{d}}_i \\ \hat{\mathbf{n}}_J \cdot \hat{\mathbf{b}}_{1_i} & \hat{\mathbf{n}}_J \cdot \hat{\mathbf{b}}_{2_i} & \hat{\mathbf{n}}_J \cdot \hat{\mathbf{d}}_i \\ \partial \mathcal{R}^\vartheta / \partial \hat{\mathbf{d}}_i \cdot \hat{\mathbf{b}}_{1_i} & \partial \mathcal{R}^\vartheta / \partial \hat{\mathbf{d}}_i \cdot \hat{\mathbf{b}}_{2_i} & \partial \mathcal{R}^\vartheta / \partial \hat{\mathbf{d}}_i \cdot \hat{\mathbf{d}}_i \end{bmatrix} \begin{Bmatrix} \delta d_1 \\ \delta d_2 \\ \delta \psi \end{Bmatrix}_{i'} = \begin{Bmatrix} 0 \\ 0 \\ -\mathcal{R}^\vartheta \end{Bmatrix} \quad (183) \end{aligned}$$

in the overall Newton system.

## 9 Newton Solution

All the discrete residuals are driven to zero by Newton iteration. For the static problem the linear Newton system for each iteration is

$$\begin{aligned} \left[ \frac{\partial \vec{\mathcal{R}}_i}{\partial \vec{v}_j} \right] \begin{Bmatrix} \delta \vec{v}_j \end{Bmatrix} &= - \begin{Bmatrix} \vec{\mathcal{R}}_i \end{Bmatrix} \\ \vec{\mathcal{R}}_i &\equiv (\mathcal{R}^{f_1}, \mathcal{R}^{f_2}, \mathcal{R}^{f_n}, \mathcal{R}^{m_1}, \mathcal{R}^{m_2}, \mathcal{R}^{m_n})_i \\ \delta \vec{v}_i &\equiv (\delta r_1, \delta r_2, \delta r_n, \delta d_1, \delta d_2, \delta \psi)_i \end{aligned} \quad (184)$$

where  $\vec{\mathcal{R}}_i$  are the projected residuals and  $\delta \vec{v}_i$  are the projected variable changes at node  $i$ . The projected Jacobian matrix  $[\partial \vec{\mathcal{R}}_i / \partial \vec{v}_j]$  is computed exactly from the current solution at each iteration. It is sparse and well conditioned due to the Poisson-type form of all the equations, and hence is well suited for iterative solution, especially for large problems.

**Nonlinear solution.** To converge a nonlinear problem, we take the undeformed geometry  $\mathbf{r}_{0,i}, \hat{\mathbf{n}}_{0,i}$  and  $\psi_i=0$  to be the initial solution guess. To perform one Newton iteration, the linear system (184) is constructed and solved, and the solution is then used to update the primary variables again using the projection vectors, possibly with an underrelaxation factor  $\omega$ .

$$\mathbf{r}_i \leftarrow \mathbf{r}_i + \omega \left( \hat{\mathbf{b}}_1^f \delta r_1 + \hat{\mathbf{b}}_2^f \delta r_2 + \hat{\mathbf{b}}_n^f \delta r_n \right)_i \quad (185)$$

$$\mathbf{d}_i \leftarrow \hat{\mathbf{d}}_i + \omega \left( \hat{\mathbf{b}}_1^m \delta d_1 + \hat{\mathbf{b}}_2^m \delta d_2 \right)_i, \quad \hat{\mathbf{d}}_i = \mathbf{d}_i / |\mathbf{d}_i| \quad (186)$$

$$\psi_i \leftarrow \psi_i + \omega \delta \psi_i \quad (187)$$

Provided there are no structural instabilities (e.g. buckling) present,  $\omega=1$  can be set and quadratic convergence is achieved. The explicit  $\mathbf{d}_i$  renormalization in (186) produces only a quadratic change in its magnitude, so it does not adversely affect the terminal quadratic convergence.

For strong geometrically nonlinear problems with large deformations,  $\omega < 1$  is typically needed initially, set either via line search, or heuristically such that the position changes do not exceed some specified fraction of the body dimensions, and that the director changes do not exceed some specified angle limit.

**Membrane sub-iteration.** For cases with thin shells and large deformations, an excessively small underrelaxation factor may be needed to stabilize the highly nonlinear iterations. A typical source of difficulty is the appearance of very large nonphysical false membrane strains and resulting stresses after a substantial deflection update, which for example can produce “transient buckling” divergence in the next iteration. A very effective fix is to temporarily freeze the director and drill variables  $\hat{\mathbf{d}}_i, \psi_i$ , and iterate only on the position variables  $\mathbf{r}_i$ , as diagrammed in Figure 11.

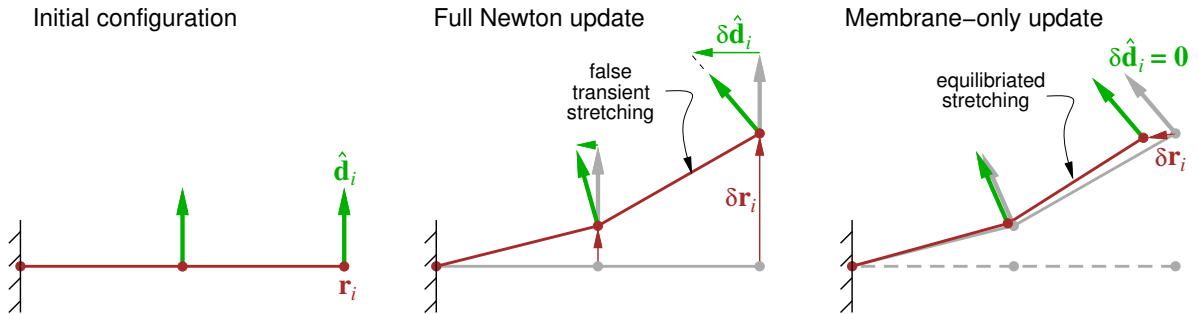


Figure 11: Non-physical membrane stretching after a large deflection Newton update is corrected with membrane-only sub-iteration, where  $\mathbf{r}_i$  is updated to obtain linear-momentum (force) equilibrium, while  $\hat{\mathbf{d}}_i$  and  $\psi_i$  are held fixed.

Specifically, we solve only the force equation and position BC equation rows in system (184) with the  $\delta d_1, \delta d_2, \delta \psi$  columns ignored, which is equivalent to forcing  $(\delta d_1, \delta d_2, \delta \psi) = (0, 0, 0)$ . We then solve only for  $\delta r_1, \delta r_2, \delta r_n$  and update  $\mathbf{r}_i$  until the force residuals are driven below a modest convergence threshold. This brings the membrane stresses to physical levels, and prevents spurious nonlinear

membrane/bending interactions for the subsequent full iteration. Since the linear system for the membrane sub-iterations is only half the size of the full system, their added computation cost is relatively minor, but the improvement in nonlinear convergence behavior is very noticable.

## 10 Unsteady Extension

### 10.1 Unsteady Variables and Equations

For dynamic problems where the shell deforms in time, the nodal primary variable vector is extended to include the node velocity vector,  $\mathbf{u}_j$ , and all variables are now functions of time.

symbol	num.	axes	description
$\mathbf{r}_j(t)$	3	$xyz$	position vector of deformed geometry
$\hat{\mathbf{d}}_j(t)$	3	$xyz$	unit material quasi-normal vector of deformed geometry
$\psi_j(t)$	1	—	drilling rotation angle
$\mathbf{u}_j(t)$	3	$xyz$	velocity vector of deformed geometry

The three new added residuals are

$$\begin{Bmatrix} \mathcal{R}_i^{u_1} \\ \mathcal{R}_i^{u_2} \\ \mathcal{R}_i^{u_n} \end{Bmatrix} \equiv \begin{bmatrix} - & \hat{\mathbf{b}}_{1_i} & - \\ - & \hat{\mathbf{b}}_{2_i} & - \\ - & \hat{\mathbf{b}}_{n_i} & - \end{bmatrix} \cdot \left\{ \dot{\mathbf{r}}_i - \mathbf{u}_i \right\} \quad (188)$$

which are in effect time-evolution ODEs for  $\mathbf{r}_i(t)$ .

The local acceleration (122) is now extended to

$$\mathbf{a} = \dot{\mathbf{U}} + \dot{\boldsymbol{\Omega}} \times \mathbf{r} + \boldsymbol{\Omega} \times (\boldsymbol{\Omega} \times \mathbf{r}) + \boldsymbol{\Omega} \times \mathbf{U} + \dot{\mathbf{u}} + 2\boldsymbol{\Omega} \times \mathbf{u} \quad (189)$$

where the new last two terms are the local frame-relative linear and Coriolis accelerations. When this is put in the force-equilibrium residuals (165), those in effect become time-evolution ODEs for the nodal  $\mathbf{u}_i(t)$  primary variables, coupled via mass matrices.

The material quasi-normal vectors  $\hat{\mathbf{d}}_i(t)$  do not have time-evolution ODEs, which is a consequence of the neglect of the mass-moment integrals  $\int \mu \zeta d\zeta \simeq 0$ ,  $\int \mu \zeta^2 d\zeta \simeq 0$ , which are thin-shell approximations. In effect, rotation of the normal vectors has no associated mass-moment of inertia, so the vectors can rotate with a zero time constant, and thus can follow the unsteady structure in a quasi-static manner.

If the mass-moment integrals were considered to be significant, then we would also need to include the frame-relative node rotation rate  $\boldsymbol{\omega}_j$  in the state vector, and this would be related to the normal-vector rate as in (189). The moment equilibrium equation would then also have an angular acceleration  $\dot{\boldsymbol{\omega}}$  term. These extensions will not be considered here.

The frame velocity vector  $\mathbf{U}(t)$  and the frame rotation vector  $\boldsymbol{\Omega}(t)$  are two additional global primary variables. Their time-evolution ODEs are obtained by applying global linear and angular momentum conservation to the entire structure,

$$\mathcal{R}^U \equiv \oint \bar{\mathbf{f}} \cdot \hat{\mathbf{t}} d\ell_0 + \iint \mathbf{q} d\mathcal{A}_0 + \iint \mu (\mathbf{g} - \mathbf{a}) d\mathcal{A}_0 \quad (190)$$

$$\mathcal{R}^\Omega \equiv \oint \mathbf{r} \times (\bar{\mathbf{f}} \cdot \hat{\mathbf{t}}) d\ell_0 + \iint \mathbf{r} \times \mathbf{q} d\mathcal{A}_0 + \iint \mu \mathbf{r} \times (\mathbf{g} - \mathbf{a}) d\mathcal{A}_0 \quad (191)$$

where the line integrals in each first term are evaluated over exposed shell edges, regardless of what boundary conditions are imposed at those edges.

## 10.2 Time-Marching

For time-marching analysis, the time derivatives are expressed in terms of the current and previous time levels using some chosen time-differencing scheme. For example, for implicit 3-point backwards differencing over time index  $n$ , with constant time steps  $\Delta t = t^n - t^{n-1} = t^{n-1} - t^{n-2}$ , we have

$$\dot{\mathbf{r}}^n = \frac{1}{2\Delta t} (3\mathbf{r}^n - 4\mathbf{r}^{n-1} + \mathbf{r}^{n-2}) \quad (192)$$

$$\dot{\mathbf{U}}^n = \frac{1}{2\Delta t} (3\mathbf{U}^n - 4\mathbf{U}^{n-1} + \mathbf{U}^{n-2}) \quad (193)$$

and likewise for  $\dot{\boldsymbol{\Omega}}^n$ . The  $n-1$  and  $n-2$  solutions have been previously computed and are known. The equations are solved by Newton iteration for the current time level  $n$  solution, and the process is then repeated for the next  $n+1$  level, thus generating a time-history sequence of solutions.

## 10.3 Perturbation Analysis

For terse notation, we first define the following overall residual, variable, and forcing vectors.

$$\vec{\mathcal{R}} = \left\{ \mathcal{R}_i^f, \mathcal{R}_i^m, \mathcal{R}_i^\theta, \mathcal{R}^U, \mathcal{R}^\Omega \right\}^\top \quad (194)$$

$$\vec{x}(t) = \left\{ \mathbf{r}_i, \hat{\mathbf{d}}_i, \psi_i, \mathbf{u}_i, \mathbf{U}, \boldsymbol{\Omega} \right\}^\top \quad (195)$$

$$\dot{\vec{x}}(t) = \left\{ \dot{\mathbf{r}}_i, \dot{\mathbf{u}}_i, \dot{\mathbf{U}}, \dot{\boldsymbol{\Omega}} \right\}^\top \quad (196)$$

$$\vec{f}(t) = \left\{ \mathbf{q}_i, \mathbf{f}_{\text{BC}_i}, \mathbf{m}_{\text{BC}_i}, \mathbf{r}_{\text{BC}_i}, \mathbf{n}_{\text{BC}_i} \right\}^\top \quad (197)$$

All the residuals can then be compactly written as

$$\vec{\mathcal{R}}(\vec{x}, \dot{\vec{x}}, \vec{f}) = \vec{0} \quad (198)$$

and we assume that these have been solved and we have a valid solution state  $\vec{x}$ . We now consider perturbations  $\delta\vec{x}(t)$ ,  $\delta\dot{\vec{x}}(t)$ ,  $\delta\vec{f}(t)$ , which are related by the linearized form of (198),

$$\delta\vec{\mathcal{R}} = \left[ \frac{\partial\vec{\mathcal{R}}}{\partial\vec{x}} \right] \delta\vec{x} + \left[ \frac{\partial\vec{\mathcal{R}}}{\partial\dot{\vec{x}}} \right] \delta\dot{\vec{x}} + \left[ \frac{\partial\vec{\mathcal{R}}}{\partial\vec{f}} \right] \delta\vec{f} = \vec{0} \quad (199)$$

where the steady, unsteady, and forcing Jacobian matrices are evaluated at the known solution. Setting the overall residual perturbation to zero in (199) imposes the requirement that the perturbed state  $\vec{x} + \delta\vec{x}$  is still a physical state to first order.

### 10.3.1 Bode analysis

Here we impose a harmonic forcing

$$\delta\vec{f} = \hat{f} \exp(i\omega t) \quad (200)$$

at some specified frequency  $\omega$ . Typically the elements of  $\hat{f}$  are all zeros, except for the single forcing element of interest which is set to unity. Alternatively, elements of  $\hat{f}$  such as  $\mathbf{q}_i$ , can have some specified spatial distribution which is modulated harmonically in time. Whatever spatial distribution  $\hat{f}$  has, the linearized solution response will be time-harmonic at the same frequency.

$$\delta\vec{x} = \hat{x} \exp(i\omega t) \quad (201)$$

$$\delta\dot{\vec{x}} = i\omega \hat{x} \exp(i\omega t) \quad (202)$$

Substituting the above perturbations into the linearized equation system (199) and rearranging gives the response vector  $\hat{x}$  explicitly.

$$\hat{x} = - \left[ \frac{\partial \vec{\mathcal{R}}}{\partial \vec{x}} + i\omega \frac{\partial \vec{\mathcal{R}}}{\partial \dot{\vec{x}}} \right]^{-1} \left[ \frac{\partial \vec{\mathcal{R}}}{\partial \vec{f}} \right] \hat{f} \quad (203)$$

Solving this complex system for a range of  $\omega$  values gives the Bode response  $\hat{x}(\omega)$  for that particular unit forcing element of  $\hat{f}$ , or spatial distribution of elements in  $\hat{f}$ .

If the structural model is strongly coupled to an aerodynamic model, the state vector  $\vec{x}$  would include the flowfield variables (e.g. grid-node velocity potentials, panel strengths, etc.), and the forcing vector  $\vec{f}$  would include atmospheric perturbation (i.e. gust) velocities. In this case, the Bode analysis of the overall system would include the complete structural response to a harmonic gust field of specified frequency and spatial distribution.

### 10.3.2 Eigenmode analysis

Here we assume no forcing

$$\delta \vec{f} = \vec{0} \quad (204)$$

and the solution is assumed to take the form

$$\delta \vec{x} = \hat{x} \exp(\lambda t) \quad (205)$$

$$\delta \dot{\vec{x}} = \lambda \hat{x} \exp(\lambda t) \quad (206)$$

where both  $\hat{x}$  and  $\lambda$  are unknown. Substituting the above perturbations into the linearized equation system (199) and rearranging gives

$$\left[ \frac{\partial \vec{\mathcal{R}}}{\partial \vec{x}} \right] \hat{x} = \lambda \left[ -\frac{\partial \vec{\mathcal{R}}}{\partial \dot{\vec{x}}} \right] \hat{x} \quad (207)$$

which is a generalized eigenvalue problem for eigenmode pairs  $\lambda, \hat{x}$ . Typical solvers for large, sparse, eigenvalue problems will return a chosen number of eigenmode pairs whose eigenvalues are closest to a specified location in the complex  $\lambda$  plane.

Instability of a mode is indicated if its real eigenvalue part is positive,  $\text{Re}(\lambda) > 0$ , and the shape of the corresponding eigenvector  $\hat{x}$  indicates the nature of this instability, such as buckling, wrinkling, etc. If the structural model is strongly coupled to an unsteady aerodynamic model, the eigenmode could be a conventional flight-dynamic instability such as spiral divergence, or an aeroelastic instability such as body-freedom flutter, or conventional twist-bending flutter.

## 11 Post-Processing Calculations

Post-processing calculations assume that a solution  $\mathbf{r}_i, \hat{\mathbf{d}}_i, \psi_i$  has been obtained. We then seek corresponding various dependent quantities at the nodes, for the purpose of graphical display or other interrogation of the solution.

### 11.1 Deformed-Geometry Nodal Basis Vectors

The nodal normal basis vectors  $\hat{\mathbf{n}}_i$  of the deformed geometry is computed via their defining residuals.

$$\mathcal{R}_i^n \equiv \iint \left[ \hat{\mathbf{n}}_i - \frac{\partial_1 \mathbf{r} \times \partial_2 \mathbf{r}}{|\partial_1 \mathbf{r} \times \partial_2 \mathbf{r}|} - \hat{\mathbf{n}}_{0_i} + \frac{\partial_1 \mathbf{r}_0 \times \partial_2 \mathbf{r}_0}{|\partial_1 \mathbf{r}_0 \times \partial_2 \mathbf{r}_0|} \right] W_i d\mathcal{A}_0 \quad (208)$$

This is linear in the one unknown vector  $\hat{\mathbf{n}}_i$ , and is independent of the unknowns at all other nodes, thus allowing a direct solution.

$$\mathcal{A}_i = \iint W_i d\mathcal{A}_0 \quad (209)$$

$$\hat{\mathbf{n}}_i = \frac{1}{\mathcal{A}_i} \iint \left[ -\frac{\partial_1 \mathbf{r} \times \partial_2 \mathbf{r}}{|\partial_1 \mathbf{r} \times \partial_2 \mathbf{r}|} - \hat{\mathbf{n}}_{0_i} + \frac{\partial_1 \mathbf{r}_0 \times \partial_2 \mathbf{r}_0}{|\partial_1 \mathbf{r}_0 \times \partial_2 \mathbf{r}_0|} \right] W_i d\mathcal{A}_0 \quad (210)$$

The nodal basis vectors  $\hat{\mathbf{e}}_1, \hat{\mathbf{e}}_2$  of the deformed geometry can be computed from the solution by first defining the element material-line vectors along the  $\xi$  coordinate lines,

$$\mathbf{s}_0 \equiv \partial_1 \mathbf{r}_0 \quad (211)$$

$$\tilde{\mathbf{s}} \equiv \partial_1 \mathbf{r} \simeq \mathbf{a}_1 \quad (212)$$

which are analogous to the shear-tilted material normal  $\hat{\mathbf{d}}$ . We also define a “shear-corrected” in-surface vector by removing from  $\tilde{\mathbf{s}}$  the in-surface tilting due to the strain tensor  $\bar{\bar{\boldsymbol{\varepsilon}}}$ ,

$$\begin{aligned} \mathbf{s} &\simeq [\bar{\mathbf{I}} - \bar{\bar{\boldsymbol{\varepsilon}}}] \cdot \tilde{\mathbf{s}} = \tilde{\mathbf{s}} - \mathbf{a}^1 (\bar{\varepsilon}_{11} \mathbf{a}^1 \cdot \mathbf{a}_1 + \bar{\varepsilon}_{12} \mathbf{a}^2 \cdot \mathbf{a}_1) - \mathbf{a}^2 (\bar{\varepsilon}_{12} \mathbf{a}^1 \cdot \mathbf{a}_1 + \bar{\varepsilon}_{22} \mathbf{a}^2 \cdot \mathbf{a}_1) \\ &= \tilde{\mathbf{s}} - \mathbf{a}^1 \bar{\varepsilon}_{11} - \mathbf{a}^2 \bar{\varepsilon}_{12} \end{aligned} \quad (213)$$

where the convenient approximation is valid for the usual small-strain case  $\varepsilon \ll 1$ .

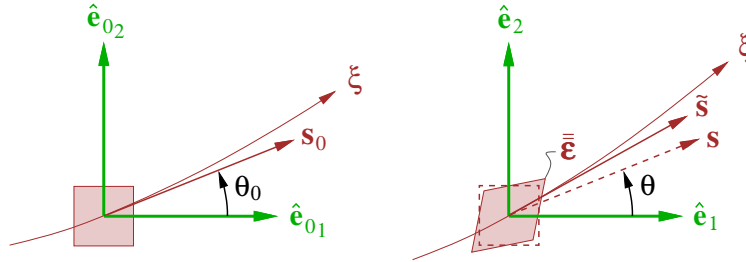


Figure 12: Top view of a small shell element for undeformed and deformed geometries, with material vectors  $\mathbf{s}_0$  and  $\tilde{\mathbf{s}}$ . Requiring  $\theta = \theta_0$  makes the  $\hat{\mathbf{e}}$  basis vectors after deformation to be fixed to the same material as  $\hat{\mathbf{e}}_0$ .

We now define the angles between these material vectors and the node basis vectors  $\hat{\mathbf{e}}_{0_1}$  and  $\hat{\mathbf{e}}_1$ .

$$\theta_0 = \text{atan2} \left( \mathbf{s}_0 \times \hat{\mathbf{e}}_{0_{1_i}} \cdot \hat{\mathbf{n}}_{0_i}, \mathbf{s}_0 \cdot \hat{\mathbf{e}}_{0_{1_i}} \right) \quad (214)$$

$$\theta = \text{atan2} \left( \mathbf{s} \times \hat{\mathbf{e}}_{1_i} \cdot \hat{\mathbf{n}}_i, \mathbf{s} \cdot \hat{\mathbf{e}}_{1_i} \right) \quad (215)$$

The three residuals defining  $\hat{\mathbf{e}}_{1_i}$  are then

$$\mathcal{R}_{1_i}^e \equiv \iint (\theta - \theta_0) \frac{W_i}{J_0^2} d\mathcal{A}_0 \quad (216)$$

$$\mathcal{R}_{2_i}^e \equiv \hat{\mathbf{e}}_{1_i} \cdot \hat{\mathbf{n}}_i \quad (217)$$

$$\mathcal{R}_{3_i}^e \equiv \hat{\mathbf{e}}_{1_i} \cdot \hat{\mathbf{e}}_{1_i} - 1 \quad (218)$$

where the  $1/J_0^2$  weighting factor makes elements which are smaller, and hence on average closer to node  $i$ , have a greater influence on the direction of  $\hat{\mathbf{e}}_{1_i}$ .

We can reduce the size of the numerical problem by projecting the unknown Newton changes onto  $\hat{\mathbf{e}}_{1_i}$ ,  $\hat{\mathbf{n}}_i$ , and  $\hat{\mathbf{e}}_{2_i} = \hat{\mathbf{n}}_i \times \hat{\mathbf{e}}_{1_i}$ ,

$$\delta \hat{\mathbf{e}}_{1_i} = \hat{\mathbf{e}}_{1_i} \delta e_1 + \hat{\mathbf{e}}_{2_i} \delta e_2 + \hat{\mathbf{n}}_i \delta e_n \quad (219)$$

and ensuring that  $\mathcal{R}_{2_i}^e = \mathcal{R}_{3_i}^e = 0$  at the start of each Newton iteration. The linearizations of residuals (217) and (218) then explicitly give  $\delta e_1 = \delta e_n = 0$ , so that only residual (216) needs to be solved for the remaining  $\delta e_2$  variable. The Newton update is performed by

$$\mathbf{e}^* = \hat{\mathbf{e}}_{1_i} + \hat{\mathbf{e}}_{2_i} \delta e_2 \quad (220)$$

$$\hat{\mathbf{e}}_{i_i} = \frac{\mathbf{e}^*}{|\mathbf{e}^*|} \quad (221)$$

$$\hat{\mathbf{e}}_{2_i} = \hat{\mathbf{n}}_i \times \hat{\mathbf{e}}_{1_i} \quad (222)$$

which ensures that  $\mathcal{R}_{2_i}^e = \mathcal{R}_{3_i}^e = 0$  as required. When the Newton iteration converges, the other surface basis vector  $\hat{\mathbf{e}}_{2_i}$  is also a by-product.

## 11.2 Nodal Strain and Stress Resultants

The HSM solution method computes the strain and stress components  $\check{\varepsilon}_{\alpha\beta}$ ,  $\check{\kappa}_{\alpha\beta}$ ,  $\check{f}^{\alpha\beta}$ ,  $\check{m}^{\alpha\beta}$ , only at the element Gauss points. To enable contour plots of the corresponding physical strain and stress quantities, it is necessary to compute the components of  $\bar{\varepsilon}$ ,  $\bar{\kappa}$ ,  $\bar{f}$ ,  $\bar{m}$  at the nodes and in the local orthonormal  $\bar{\mathbf{e}}_0$  basis. Suppressing the  $( )_0$  subscripts for clarity, we equate the node-basis and element-basis forms of the in-surface strain resultant tensor,

$$\begin{aligned} \sum_j \bar{\varepsilon}_j N_j &= \check{\varepsilon}_{\alpha\beta} \mathbf{a}^\alpha \mathbf{a}^\beta \\ \sum_j \left[ \varepsilon_{11j} \hat{\mathbf{e}}_{1_j} \hat{\mathbf{e}}_{1_j} + \varepsilon_{12j} (\hat{\mathbf{e}}_{1_j} \hat{\mathbf{e}}_{2_j} + \hat{\mathbf{e}}_{2_j} \hat{\mathbf{e}}_{1_j}) + \varepsilon_{22j} \hat{\mathbf{e}}_{2_j} \hat{\mathbf{e}}_{2_j} \right] N_j \\ &= \check{\varepsilon}_{11} \mathbf{a}^1 \mathbf{a}^1 + \check{\varepsilon}_{12} (\mathbf{a}^1 \mathbf{a}^2 + \mathbf{a}^2 \mathbf{a}^1) + \check{\varepsilon}_{22} \mathbf{a}^2 \mathbf{a}^2 \end{aligned} \quad (223)$$

where the node-basis form has been interpolated to the element interior. To construct the discrete residuals, we form the dot products of the above equation's residual with the basis vectors of a node  $i$ , and integrate the resulting expressions with the  $W_i$  weighting function of that node, e.g.

$$\mathcal{R}_i^{\varepsilon_{12}} \equiv \iint \hat{\mathbf{e}}_{1_i} \cdot \left\{ \sum_j \bar{\varepsilon}_j N_j - \check{\varepsilon}_{\alpha\beta} \mathbf{a}^\alpha \mathbf{a}^\beta \right\} \cdot \hat{\mathbf{e}}_{2_i} W_i \, d\mathcal{A}_0$$

Picking the  $(\hat{\mathbf{e}}_{1_i}, \hat{\mathbf{e}}_{1_i})$ ,  $(\hat{\mathbf{e}}_{2_i}, \hat{\mathbf{e}}_{2_i})$ ,  $(\hat{\mathbf{e}}_{1_i}, \hat{\mathbf{e}}_{2_i})$  vector pairs in the definition above defines the residuals for the three strain components  $\varepsilon_{11}, \varepsilon_{22}, \varepsilon_{12}$  of node  $i$ .

$$\mathcal{R}_i^{\varepsilon_{11}} \equiv \iint \sum_j \hat{\mathbf{e}}_{1_i} \cdot \bar{\varepsilon}_j \cdot \hat{\mathbf{e}}_{1_i} N_j W_i \, d\mathcal{A}_0 - \iint \check{\varepsilon}_{\alpha\beta} (\hat{\mathbf{e}}_{1_i} \cdot \mathbf{a}^\alpha) (\hat{\mathbf{e}}_{1_i} \cdot \mathbf{a}^\beta) W_i \, d\mathcal{A}_0 \quad (224)$$

$$\mathcal{R}_i^{\varepsilon_{22}} \equiv \iint \sum_j \hat{\mathbf{e}}_{2_i} \cdot \bar{\varepsilon}_j \cdot \hat{\mathbf{e}}_{2_i} N_j W_i \, d\mathcal{A}_0 - \iint \check{\varepsilon}_{\alpha\beta} (\hat{\mathbf{e}}_{2_i} \cdot \mathbf{a}^\alpha) (\hat{\mathbf{e}}_{2_i} \cdot \mathbf{a}^\beta) W_i \, d\mathcal{A}_0 \quad (225)$$

$$\mathcal{R}_i^{\varepsilon_{12}} \equiv \iint \sum_j \hat{\mathbf{e}}_{1_i} \cdot \bar{\varepsilon}_j \cdot \hat{\mathbf{e}}_{2_i} N_j W_i \, d\mathcal{A}_0 - \iint \check{\varepsilon}_{\alpha\beta} (\hat{\mathbf{e}}_{1_i} \cdot \mathbf{a}^\alpha) (\hat{\mathbf{e}}_{2_i} \cdot \mathbf{a}^\beta) W_i \, d\mathcal{A}_0 \quad (226)$$

Each integral consists of four terms. For example, in (226) we have

$$\begin{aligned}\hat{\mathbf{e}}_{1_i} \cdot \bar{\bar{\mathbf{e}}}_j \cdot \hat{\mathbf{e}}_{2_i} &:= \varepsilon_{11j}(\hat{\mathbf{e}}_{1_i} \cdot \hat{\mathbf{e}}_{1_j})(\hat{\mathbf{e}}_{2_i} \cdot \hat{\mathbf{e}}_{1_j}) \\ &+ \varepsilon_{12j}(\hat{\mathbf{e}}_{1_i} \cdot \hat{\mathbf{e}}_{1_j})(\hat{\mathbf{e}}_{2_i} \cdot \hat{\mathbf{e}}_{2_j}) \\ &+ \varepsilon_{21j}(\hat{\mathbf{e}}_{1_i} \cdot \hat{\mathbf{e}}_{2_j})(\hat{\mathbf{e}}_{2_i} \cdot \hat{\mathbf{e}}_{1_j}) \\ &+ \varepsilon_{22j}(\hat{\mathbf{e}}_{1_i} \cdot \hat{\mathbf{e}}_{2_j})(\hat{\mathbf{e}}_{2_i} \cdot \hat{\mathbf{e}}_{2_j})\end{aligned}\quad (227)$$

and summing over  $\alpha, \beta$  in the second integral likewise produces four terms.

$$\begin{aligned}\check{\varepsilon}_{\alpha\beta}(\hat{\mathbf{e}}_{1_i} \cdot \mathbf{a}^\alpha)(\hat{\mathbf{e}}_{2_i} \cdot \mathbf{a}^\beta) &:= \check{\varepsilon}_{11}(\hat{\mathbf{e}}_{1_i} \cdot \mathbf{a}^1)(\hat{\mathbf{e}}_{2_i} \cdot \mathbf{a}^1) \\ &+ \check{\varepsilon}_{12}(\hat{\mathbf{e}}_{1_i} \cdot \mathbf{a}^1)(\hat{\mathbf{e}}_{2_i} \cdot \mathbf{a}^2) \\ &+ \check{\varepsilon}_{21}(\hat{\mathbf{e}}_{1_i} \cdot \mathbf{a}^2)(\hat{\mathbf{e}}_{2_i} \cdot \mathbf{a}^1) \\ &+ \check{\varepsilon}_{22}(\hat{\mathbf{e}}_{1_i} \cdot \mathbf{a}^2)(\hat{\mathbf{e}}_{2_i} \cdot \mathbf{a}^2)\end{aligned}\quad (228)$$

The same procedure is used to obtain the residuals which determine the curvature-change components  $\kappa_{11}, \kappa_{12}, \kappa_{22}$  of node  $i$ .

$$\mathcal{R}_i^{\kappa_{11}} \equiv \iint \sum_j \hat{\mathbf{e}}_{1_i} \cdot \bar{\bar{\mathbf{\kappa}}}_j \cdot \hat{\mathbf{e}}_{1_i} N_j W_i \, d\mathcal{A}_0 - \iint \check{\kappa}_{\alpha\beta}(\hat{\mathbf{e}}_{1_i} \cdot \mathbf{a}^\alpha)(\hat{\mathbf{e}}_{1_i} \cdot \mathbf{a}^\beta) W_i \, d\mathcal{A}_0 \quad (229)$$

$$\mathcal{R}_i^{\kappa_{22}} \equiv \iint \sum_j \hat{\mathbf{e}}_{2_i} \cdot \bar{\bar{\mathbf{\kappa}}}_j \cdot \hat{\mathbf{e}}_{2_i} N_j W_i \, d\mathcal{A}_0 - \iint \check{\kappa}_{\alpha\beta}(\hat{\mathbf{e}}_{2_i} \cdot \mathbf{a}^\alpha)(\hat{\mathbf{e}}_{2_i} \cdot \mathbf{a}^\beta) W_i \, d\mathcal{A}_0 \quad (230)$$

$$\mathcal{R}_i^{\kappa_{12}} \equiv \iint \sum_j \hat{\mathbf{e}}_{1_i} \cdot \bar{\bar{\mathbf{\kappa}}}_j \cdot \hat{\mathbf{e}}_{2_i} N_j W_i \, d\mathcal{A}_0 - \iint \check{\kappa}_{\alpha\beta}(\hat{\mathbf{e}}_{1_i} \cdot \mathbf{a}^\alpha)(\hat{\mathbf{e}}_{2_i} \cdot \mathbf{a}^\beta) W_i \, d\mathcal{A}_0 \quad (231)$$

To obtain the nodal stress and stress-moment resultants, we follow the procedure above, except that the covariant element basis vectors are now used. For example the residual for  $f_{11i}$  is

$$\mathcal{R}_i^{f_{11}} \equiv \iint \sum_j \hat{\mathbf{e}}_{1_i} \cdot \bar{\bar{\mathbf{f}}}_j \cdot \hat{\mathbf{e}}_{1_i} N_j W_i \, d\mathcal{A}_0 - \iint \check{f}^{\alpha\beta}(\hat{\mathbf{e}}_{1_i} \cdot \mathbf{a}_\alpha)(\hat{\mathbf{e}}_{1_i} \cdot \mathbf{a}_\beta) W_i \, d\mathcal{A}_0 \quad (232)$$

which has the same form as (224) except that  $\mathbf{a}^\alpha, \mathbf{a}^\beta$  have been replaced by  $\mathbf{a}_\alpha, \mathbf{a}_\beta$ .

All the residual equations above are linear in the nodal variables, and can be written as

$$\left[ A_{ij} \right] \left\{ \begin{array}{c} \bar{\bar{\varepsilon}}_j \\ \bar{\bar{\kappa}}_j \\ \bar{\bar{f}}_j \\ \bar{\bar{m}}_j \end{array} \right\} = \left\{ \begin{array}{c} \bar{\bar{\mathcal{R}}}_i^\varepsilon \\ \bar{\bar{\mathcal{R}}}_i^\kappa \\ \bar{\bar{\mathcal{R}}}_i^f \\ \bar{\bar{\mathcal{R}}}_i^m \end{array} \right\} \quad (233)$$

where the unknown symmetric tensors are arranged in vector form, e.g.  $\bar{\bar{\varepsilon}}_j = (\varepsilon_{11}, \varepsilon_{22}, \varepsilon_{12})_j$ , and their residuals are arranged the same way and evaluated with the nodal unknowns ignored. The common mass matrix  $A_{ij}$  depends only on the undeformed geometry  $\mathbf{r}_{0_i}$  and the chosen  $\bar{\bar{\mathbf{e}}}_{0_i}$  basis vectors. Hence,  $A_{ij}$  needs to be LU-factored only once a-priori, and can then be used to rapidly determine all the nodal tensor quantities for any solution for that geometry.

The same procedure is also used to obtain the residuals for the two transverse shear strain and stress components  $\gamma_1, \gamma_2, f_{1n}, f_{2n}$  of node  $i$ .

$$\mathcal{R}_i^{\gamma_1} \equiv \iint \sum_j \hat{\mathbf{e}}_{1_i} \cdot \gamma_j N_j W_i \, d\mathcal{A}_0 - \iint \check{\gamma}_\alpha(\hat{\mathbf{e}}_{1_i} \cdot \mathbf{a}^\alpha) W_i \, d\mathcal{A}_0 \quad (234)$$

$$\mathcal{R}_i^{\gamma_2} \equiv \iint \sum_j \hat{\mathbf{e}}_{2_i} \cdot \gamma_j N_j W_i \, d\mathcal{A}_0 - \iint \check{\gamma}_\alpha(\hat{\mathbf{e}}_{2_i} \cdot \mathbf{a}^\alpha) W_i \, d\mathcal{A}_0 \quad (235)$$

$$\mathcal{R}_i^{f_{1n}} \equiv \iint \sum_j \hat{\mathbf{e}}_{1_i} \cdot \mathbf{f}_{n_j} N_j W_i \, d\mathcal{A}_0 - \iint \check{f}^{\alpha n}(\hat{\mathbf{e}}_{1_i} \cdot \mathbf{a}_\alpha) W_i \, d\mathcal{A}_0 \quad (236)$$

$$\mathcal{R}_i^{f_{2n}} \equiv \iint \sum_j \hat{\mathbf{e}}_{2_i} \cdot \mathbf{f}_{n_j} N_j W_i \, d\mathcal{A}_0 - \iint \check{f}^{\alpha n}(\hat{\mathbf{e}}_{2_i} \cdot \mathbf{a}_\alpha) W_i \, d\mathcal{A}_0 \quad (237)$$



Expanding the dot product in the first integral and summing over  $\alpha$  in the second integral gives

$$\begin{aligned}\hat{\mathbf{e}}_{1_i} \cdot \mathbf{f}_{n_j} &:= f_{1n_j}(\hat{\mathbf{e}}_{1_i} \cdot \hat{\mathbf{e}}_{1_j}) \\ &+ f_{2n_j}(\hat{\mathbf{e}}_{1_i} \cdot \hat{\mathbf{e}}_{2_j})\end{aligned}\quad (238)$$

$$\begin{aligned}\check{f}^{\alpha n}(\hat{\mathbf{e}}_{1_i} \cdot \mathbf{a}_\alpha) &:= \check{f}^{1n}(\hat{\mathbf{e}}_{1_i} \cdot \mathbf{a}_1) \\ &+ \check{f}^{2n}(\hat{\mathbf{e}}_{1_i} \cdot \mathbf{a}_2)\end{aligned}\quad (239)$$

which compared to (227) and (228) has only the single dot products since here we are working with vectors rather than tensors. The residual equations can be put into the form of the linear system

$$\left[ B_{ij} \right] \left\{ \vec{\gamma}_j \mid \vec{f}_{n_j} \right\} = \left\{ \vec{\mathcal{R}}_i^\gamma \mid \vec{\mathcal{R}}_i^{f_n} \right\} \quad (240)$$

where as in the tensor system (233), the common mass matrix  $B_{ij}$  depends only on the undeformed geometry and its  $\bar{\mathbf{e}}_{0_i}$  vectors.

### 11.3 Maximum Strain and Stress

The extremal in-surface strain within the shell will occur on its surface, where the strain tensor is given by (58)

$$\begin{Bmatrix} \varepsilon'_{11} \\ \varepsilon'_{22} \\ \varepsilon'_{12} \end{Bmatrix} = \begin{Bmatrix} \varepsilon_{11} \\ \varepsilon_{22} \\ \varepsilon_{12} \end{Bmatrix} + \zeta \begin{Bmatrix} \kappa_{11} \\ \kappa_{22} \\ \kappa_{12} \end{Bmatrix} \quad (241)$$

where we set  $\zeta = \zeta_{\text{top}}$  and then  $\zeta = \zeta_{\text{bot}}$  to examine both the top and bottom surfaces. To gauge failure of a composite shell material, these strains would typically be compared with that material's maximum allowable normal and shear strains in the 12 axes.

For an isotropic shell material with modulus  $E$  and Poisson's ratio  $\nu$  it is useful to instead examine the corresponding stresses via the isotropic stiffness tensor,

$$\begin{Bmatrix} \sigma_{11} \\ \sigma_{22} \\ \sigma_{12} \end{Bmatrix} = \frac{E}{1-\nu^2} \begin{bmatrix} 1 & \nu & 0 \\ \nu & 1 & 0 \\ 0 & 0 & 1-\nu \end{bmatrix} \begin{Bmatrix} \varepsilon'_{11} \\ \varepsilon'_{22} \\ \varepsilon'_{12} \end{Bmatrix} \quad (242)$$

The surface principal stress values are then given by

$$\bar{\sigma}_1 = \frac{1}{2}(\sigma_{11} + \sigma_{22}) + \sqrt{\frac{1}{4}(\sigma_{11} - \sigma_{22})^2 + \sigma_{12}^2} \quad (243)$$

$$\bar{\sigma}_2 = \frac{1}{2}(\sigma_{11} + \sigma_{22}) - \sqrt{\frac{1}{4}(\sigma_{11} - \sigma_{22})^2 + \sigma_{12}^2} \quad (244)$$

and these then give the vonMises stress.

$$\sigma_e = \sqrt{\bar{\sigma}_1^2 + \bar{\sigma}_2^2 - \bar{\sigma}_1 \bar{\sigma}_2} \quad (245)$$

The ratio  $\sigma_e/\sigma_y$ , where  $\sigma_y$  is the material's yield stress, is a useful yield-margin indicator. Again, both the top and bottom surfaces of the shell would need to be examined separately.

## 12 Stiffness Matrix Specification

### 12.1 General and shell constitutive relations

For a Hookean material, the stress tensor components are related to the strain tensor components via the stiffness tensor  $c_{ijkl}$  defined in the local  $12n$  axes, so that each of the four indices can take on the three values  $i, j, k, l \in [1, 2, n]$ . Voigt-type notation is used to contract the index pairs as

$$()_{11} \rightarrow ()_1, \quad ()_{22} \rightarrow ()_2, \quad ()_{nn} \rightarrow ()_3, \quad ()_{2n} \rightarrow ()_4, \quad ()_{1n} \rightarrow ()_5, \quad ()_{12} \rightarrow ()_6$$

so for example  $c_{1122} \rightarrow c_{12}$  and  $c_{2n2n} \rightarrow c_{44}$ . The general Hookean constitutive relations are then

$$\begin{Bmatrix} \sigma_{11} \\ \sigma_{22} \\ \sigma_{nn} \\ \sigma_{2n} \\ \sigma_{1n} \\ \sigma_{12} \end{Bmatrix} = \begin{bmatrix} c_{11} & c_{12} & c_{13} & c_{14} & c_{15} & c_{16} \\ \cdot & c_{22} & c_{23} & c_{24} & c_{25} & c_{26} \\ \cdot & \cdot & c_{33} & c_{34} & c_{35} & c_{36} \\ \cdot & \cdot & \cdot & c_{44} & c_{45} & c_{46} \\ \cdot & \cdot & \cdot & \cdot & c_{55} & c_{56} \\ \cdot & \cdot & \cdot & \cdot & \cdot & c_{66} \end{bmatrix} \begin{Bmatrix} \varepsilon_{11} \\ \varepsilon_{22} \\ \varepsilon_{nn} \\ \varepsilon_{2n} \\ \varepsilon_{1n} \\ \varepsilon_{12} \end{Bmatrix} \quad (246)$$

which with the indicated symmetry has 21 independent stiffness constants. The symmetry follows from the conservation of angular momentum, specifically the requirement of a bounded torque/inertia ratio for an arbitrarily small volume.

The general relation (246) is considerably simplified using the shell assumptions that  $\sigma_{nn}$  and  $\varepsilon_{nn}$  are negligible, and that the in-surface stress tensor components  $\sigma_{11}, \sigma_{22}, \sigma_{12}$  are decoupled from the transverse components  $\sigma_{1n}, \sigma_{2n}$ . Relation (246) thus reduces to

$$\begin{Bmatrix} \sigma_{11} \\ \sigma_{22} \\ \sigma_{12} \end{Bmatrix} = \begin{bmatrix} c_{11} & c_{12} & c_{16} \\ \cdot & c_{22} & c_{26} \\ \cdot & \cdot & c_{66} \end{bmatrix} \begin{Bmatrix} \varepsilon_{11} \\ \varepsilon_{22} \\ \varepsilon_{12} \end{Bmatrix} \quad (247)$$

$$\begin{Bmatrix} \sigma_{1n} \\ \sigma_{2n} \end{Bmatrix} = \begin{bmatrix} c_{55} & 0 \\ 0 & c_{44} \end{bmatrix} \begin{Bmatrix} \gamma_1 \\ \gamma_2 \end{Bmatrix} \quad (248)$$

$$\sigma_{nn} = 0 \quad (249)$$

which now has only 8 stiffness constants. This is the same as (56) and (57) aside from the distinction between  $\varepsilon'$  and  $\varepsilon$  which is not relevant here.

### 12.2 Isotropic material properties

An isotropic Hookean shell material is characterized only by the modulus  $E$  and Poisson's ratio  $\nu$ , which give all the stiffness matrix components as follows.

$$\begin{bmatrix} c_{11} & c_{12} & c_{16} \\ & c_{22} & c_{26} \\ & & c_{66} \end{bmatrix} = \frac{E}{1-\nu^2} \begin{bmatrix} 1 & \nu & 0 \\ & 1 & 0 \\ & & 1-\nu \end{bmatrix} \quad (250)$$

$$\begin{bmatrix} c_{55} \\ c_{44} \end{bmatrix} = \frac{E}{2(1+\nu)} \begin{bmatrix} 1 & \\ & 1 \end{bmatrix} \quad (251)$$

### 12.3 Orthotropic material properties

An orthotropic shell material has in-surface moduli  $E_1, E_2, G_{12}$  and Poisson's ratio  $\nu_{12}$ , and transverse shear moduli  $G_{13}, G_{23}$ . The material stiffness and compliance matrix elements are then given as follows.

$$\begin{bmatrix} c_{11} & c_{12} & c_{16} \\ & c_{22} & c_{26} \\ & & c_{66} \end{bmatrix} = \frac{1}{1-\nu^2} \begin{bmatrix} E_1 & E_2 \nu_{12} & 0 \\ & E_2 & 0 \\ & & 2G_{12}(1-\nu^2) \end{bmatrix}, \quad \nu^2 \equiv \nu_{12}^2 E_2 / E_1 \quad (252)$$

$$\begin{bmatrix} c_{55} \\ & c_{44} \end{bmatrix} = \begin{bmatrix} G_{13} \\ & G_{23} \end{bmatrix} \quad (253)$$

### 12.4 Resultant stiffness matrix calculation

The reference-surface location  $\zeta_{\text{ref}}$  within the shell thickness  $h = \zeta_{\text{top}} - \zeta_{\text{bot}}$  is conveniently specified by the fractional  $\bar{\zeta}_{\text{ref}} \equiv \zeta_{\text{ref}}/2h$  parameter, so that  $\bar{\zeta}_{\text{ref}} = -1, 0, +1$  indicates bottom, middle, and top locations, respectively, or anything else in between.

$$\zeta_{\text{ref}} = \frac{1}{2}(1-\bar{\zeta}_{\text{ref}})\zeta_{\text{bot}} + \frac{1}{2}(1+\bar{\zeta}_{\text{ref}})\zeta_{\text{top}} \quad (254)$$

For an isotropic or orthotropic shell material, the integrals in (62)–(65) can be evaluated to explicitly give the following shell stiffness matrices.

$$\bar{\bar{A}} = h \bar{\bar{c}} \quad (255)$$

$$\bar{\bar{B}} = -h^2 \frac{\bar{\zeta}_{\text{ref}}}{2} \bar{\bar{c}} \quad (256)$$

$$\bar{\bar{D}} = h^3 \frac{1 + 3\bar{\zeta}_{\text{ref}}^2}{12} \bar{\bar{c}} \quad (257)$$

$$\bar{\bar{S}} = Kh \bar{\bar{s}} \quad (258)$$

The stiffness matrices of composite-laminate shells can be computed using laminate theory, whose inputs are the thickness, angle, and orthotropic material constants  $E_1, E_2, G_{12}, \nu_{12}$  of each of the individual composite plies in the stack. A balanced composite laminate will behave as a uniform orthotropic (or isotropic in special cases) material with some net effective  $\bar{E}_1, \bar{E}_2, \bar{G}_{12}, \bar{\nu}_{12}$  parameters. Unbalanced laminates have nonzero  $A_{16}$  and  $A_{26}$  constants, which produce extension/shear coupling. Asymmetric laminates will have nonzero  $B_{16}$  and  $B_{26}$  constants, which produce extension/twist coupling. Laminates which are either unbalanced or asymmetric will have nonzero  $D_{16}$  and  $D_{26}$  constants, which produce bending/twist coupling.

### 12.5 Lumped-structure shells

One advantage of a shell model is that it can approximate the behavior of a relatively complex structure with stringers, doublers, etc. by a monolithic shell with equivalent stiffnesses. This monolithic shell requires much fewer parameters to describe, and is therefore better suited for early design and optimization, or if the structure is driven by and coupled with an aerodynamic solver.

To perform the lumping, the mass, stress, and stiffness definition integrals (12) and (62)–(65) over the thickness are then extended to include averaging over parts of the surface. For example, for a shell structure with stiffeners running in the spanwise direction, a suitable lumped stiffness is

$$\bar{\bar{A}}(t) = \begin{bmatrix} A_{11} & A_{12} & A_{16} \\ \cdot & A_{22} & A_{26} \\ \cdot & \cdot & A_{66} \end{bmatrix} \equiv \frac{1}{\Delta t} \int_{t-\Delta t/2}^{t+\Delta t/2} \int_{\zeta_{\text{bot}}}^{\zeta_{\text{top}}} \begin{bmatrix} c_{11} & c_{12} & c_{16} \\ \cdot & c_{22} & c_{26} \\ \cdot & \cdot & c_{66} \end{bmatrix}_{(\zeta, t')} d\zeta dt' \quad (259)$$

where a natural transverse-averaging interval  $\Delta t$  would be the stringer spacing distance, as shown in Figure 13. The averaging interval could even be the entire transverse width, giving a transversely-uniform equivalent lumped shell.

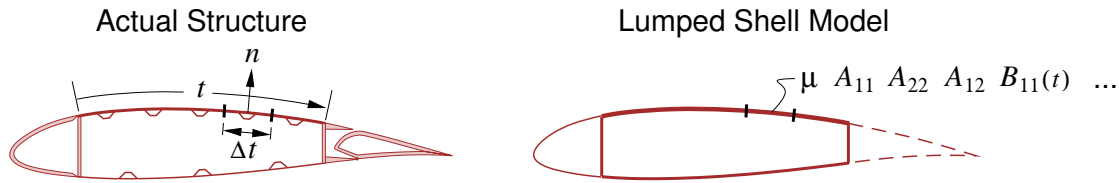


Figure 13: Complex shell structure can be lumped into a simpler equivalent monolithic shell, defined by transverse averaging integration over some interval  $\Delta t$ .

## References

- [1] S. Ahmad, B.M. Irons, and O.C. Zienkewicz. Analysis of thick and thin shell structures by curved finite elements. *Int. J. Num. Meth. Eng.*, 2:419–451, 1970.
- [2] Jr. Sanders, J.L. Nonlinear theories for thin shells. Technical Report 10, Division of Engineering and Applied Physics, Harvard University, Feb 1961.
- [3] E.N. Dvorkin and K.J. Bathe. A continuum mechanics based fournode shell element for general nonlinear analysis. *Engineering Computations*, 1(1):77–88, 1984.
- [4] J.C. Simo and D.D. Fox. On a stress resultant geometrically exact shell model. Part I: Formulation and optimal parametrization. *Computer Meth. in Appl. Mechanics and Eng.*, 72:267–304, 1989.
- [5] J.C. Simo, D.D. Fox, and M.S. Rifai. On a stress resultant geometrically exact shell model. Part III: Computational aspects of the nonlinear theory. *Computer Meth. in Appl. Mechanics and Eng.*, 79:21–70, 1990.
- [6] B.L. Talamini and R. Radovitzky. A discontinuous galerkin method for nonlinear shear-flexible shells. *Comput. Methods Appl. Mech. Engrg.*, 303:128–162, 2016.
- [7] A. Ibrahimbegović. Stress resultant geometrically nonlinear shell theory with drilling rotations — Part I. a consistent formulation. *Computer Meth. in Appl. Mechanics and Eng.*, 118:265–284, 1994.
- [8] Y. Lee, P.S. Lee, and K.J. Bathe. The MITC3+ shell element and its performance. *Computers and Structures*, 138:12–38, 2014.
- [9] J.C. Simo, D.D. Fox, and M.S. Rifai. On a stress resultant geometrically exact shell model. Part II: The linear theory; computational aspects. *Computer Meth. in Appl. Mechanics and Eng.*, 73:53–92, 1989.